SACLANTCEN REPORT
serial no: SR-295

SACLANT UNDERSEA
RESEARCH CENTRE
REPORT

RESONANCE ANALYSIS OF THE ACOUSTIC RESPONSE OF A WATER-FILLED CYLINDRICAL SHELL

A. Tesei, J.A. Fawcett, W.L.J. Fox, A Maguer

September 1998

Report no. changed (Mar 2006): SR-295-UU

SACLANT Undersea Research Centre
Viale San Bartolomeo 400
19138 San Bartolomeo (SP), Italy

tel: +39-0187-540.111
fax: +39-0187-524.600

e-mail: library@saclantc.nato.int

NORTH ATLANTIC TREATY ORGANIZATION

Resonance analysis of the acoustic response of a water-filled cylindrical shell

A. Tesei, J. A. Fawcett,
W. L. J. Fox, A. Maguer

The content of this document pertains to work performed under Projects 031-2 and 033-3 of the SACLANTCEN Programme of Work. The document has been approved for release by The Director, SACLANTCEN.

Jan L. Spoelstra
Director

Resonance analysis of the acoustic response of a water-filled cylindrical shell

A. Tesei, J. A. Fawcett, W. L. J. Fox,
A. Maguer

Executive Summary:

Conventional mine classification systems use high frequency, high resolution sonar methods to obtain acoustic "pictures" of mine-like objects and their acoustic "shadows" in order to classify them. In order to extend classification ability for proud (resting on the seabed), partially buried, and completely buried objects, lower frequency broad band methods are being investigated. This report deals with extraction and identification of *resonance* phenomena from target signatures in order to infer some of the physical properties of these objects. The resonance phenomena are due to periodic waves traveling around and inside an acoustically excited elastic object. Location in frequency is directly related to parameters of the object.

Earlier work concentrated on air-filled cylindrical shells, which allowed prototyping of resonance extraction and parameter identification methodologies for a relatively simple and well understood case. This report extends those results for the water-filled case. Although well understood theoretically, this case poses a greater challenge for the algorithms of feature selection and extraction due to the more complicated nature of the resonance structure. Obtaining a better understanding of these canonical targets is an important precursor for applying the methods to targets encountered operationally.

In free space, given some knowledge of an object's external shape, it is possible to characterize the shell wall thickness and material properties, and the properties of the inner medium. This report also addresses the influence of a boundary on resonance for the case when an object is resting on the seabed. It is found that for certain conditions of transmit/receive geometry, the characterization methodology developed for the free space case is also applicable. The algorithm is tested on model-based and high-SNR experimental data with good results, giving confidence that the theoretical interpretation proposed here is valid.

Future work will concentrate on extending these results to partially and completely buried shells, and to determining performance as a function of SNR. Responses of real mines, other man-made objects, and natural objects will also be examined.

intentionally blank page

intentionally blank page

Resonance analysis of the acoustic response of a water-filled cylindrical shell

A. Tesei, J. A. Fawcett, W. L. J. Fox,
A. Maguer

Abstract:

The resonance analysis approach developed for characterizing free-field air-filled cylindrical shells in terms of geometrical and mechanical parameters is extended to fluid-filled shells either in the free-field or proud on the sea bottom.

The resonance phenomena generated when a target is insonified at broadside, by broadband, low-frequency, incident pulses are investigated in the *ka* range (2,25). Attention is focused on those scattering phenomena common to free-field and proud cases. A comparison is also drawn between the resonance behavior of the same cylindrical target filled with either air or sea water. From the study of a set of fluid-borne and shell-borne wave families, equations are formulated which relate their characteristics to the target elastic properties. Resonance frequencies are detected and localized by the algorithm presented earlier, identified and used for parameter estimation by an automatic multi-hypothesis method of model-data fitting. The approach was tested on real acoustic data backscattered by a water-filled finite cylinder either suspended in free-field, or lying proud on a sandy sea bottom and insonified at very low grazing angle (below the seabed critical angle). A good agreement between theory and experiment was found in terms of model-data fit and target parameter estimates.

The results achieved encourage the extension of target echo analysis to objects buried in bottom sediment. The extension to multi-aspect resonance scattering analysis of the same and more complex objects is also planned.

Keywords: sound scattering ◦ elastic cylinders ◦ resonance analysis

Contents

1

Introduction

Recent research at SACLANTCEN has focused on broadband low-frequency sonars for minehunting applications in the low-intermediate *ka* range (2,20). At these frequencies the resonance scattering contribution by an elastic object is significant and can provide useful information on geometrical and mechanical properties, on which the resonance characteristics depend. The broadband (in the sense of large relative bandwidth) nature of these sonars allows the extraction of target classification clues.

This approach can be useful for minehunting, when mines are proud on the sea bottom in high-clutter density areas, where detection results generally present high false alarm rates. Under these conditions, the low-intermediate frequency broadband methodology may be helpful for excluding non-minelike objects from consideration (e.g., mine-sized rocks) because of their non-elastic scattering behavior. An extension of the approach could include the classification of buried mines, as the low-frequency bandwidth facilitates sound propagation into bottom sediments.

Theoretical and experimental work has been performed at SACLANTCEN on scattering by elastic, simple-shaped targets insonified by broadband low-frequency pulses in free field and proud on the sea bottom. Measured free-field scattering, by thin-walled cylindrical shells at broadside, was shown to match well with selected theoretical models, in the *ka* range (4-16), based on Resonance Scattering Theory (RST) [1][2]. Responses by the same shell filled with different fluids (i.e., air and sea water) were significantly different in time and frequency domains.

On the basis of these preliminary considerations and previous studies [2][3], Tesei et al. [4] addressed the study and physical interpretation of surface wave families scattered by an air-filled thin-walled cylindrical shell insonified at broadside in the free field. This led to the formulation of analytical models to match target elastic properties with scattered resonance characteristics. Scattered data [1] were analyzed by AR-based signal processing techniques in the *ka* range (2,50). Application of the matching models resulted in accurate estimates of target parameters (e.g., shell inner and outer radii and shell material), given some *a priori* information.

In [5] a theoretical model of scattering by elastic cylindrical and spherical objects lying proud on a seabed was proposed. The model was validated by matching with real data scattered by an aluminum sphere and by the same water-filled cylindrical

shell used in [1]. The agreement between theory and experiment appeared good in terms of response curve fitting, in the time and frequency domains. In [6] this model was extended to objects partially buried in a seabed, in conclusion with more realistic assumptions about the influence of the sea bottom.

This report extends the study of the resonance contribution scattered by an air-filled cylindrical shell in the free-field [4] to the case of generically fluid-filled, cylindrical shells, at broadside in free field and proud on a seabed. As in [4], resonance modes are extracted by autoregressive (AR) techniques [7] and identified through further processing.

Theory shows that scattered acoustic pressure consists of two main contributions: a non-resonant background, smoothly varying with frequency, and a resonance component. The latter consists of a series of echoes corresponding to resonance frequencies, which generally appear in the scatterer form function curve as dips, peaks or non-derivative points occurring at frequencies very close to natural frequencies (i.e., eigenfrequencies) of the elastic target. Resonance scattering theory is the study of the relation between resonance frequencies detected in the scatterer form function and the surface waves traveling around the target [8]. Conventionally [2], the resonance frequency f_n of modal order n occurs when the radius R of the object circular cross-section around which the wave W travels is equal to an integer number n of its wavelength λ^W:

$$2\pi R = n\lambda^W. \tag{1}$$

Good agreement between theory and experiment has been found for solid, elastic, simple-shaped objects such as cylinders at broadside and spheres [9][10]. For thin elastic shells, the interpretation of experimental data on the basis of theory is more difficult and has given rise to numerous hypotheses, partially from analogy with the study of thin infinite plates either dry or fluid-loaded on one or both sides. As a first analysis step, in [4] the main families of circumferential waves backscattered by an air-filled shell at broadside were interpreted according to the theories proposed in [2], [8], and cited works.

For generic liquid-filled shells, the problem is open, in particular when the liquid filling the shell is different to that loading it. Previous work [11][12] on fluid-loaded, thin plates and fluid-filled shells have proposed the existence of many types of fluid- and shell-borne resonance families.

The theoretical study presented in this report is based on scattering models derived from RST [3] and Plane Plate Theory (PPT) [13][14] for the free-space, and by the Single Scattering (SSC) model [5] for the proud case. Several wave types either described in the cited works or introduced here are investigated, characterized through their dispersion curves, interpreted and related to resonance features detected and localized in the scatterer frequency response. Every acoustic wave backscattered

periodically by an insonified target is assumed to give rise to *resonance*. Hence the term is intended in a wider sense than the definition of Eq. (1), including *surface* not only waves traveling at the fluid-shell interfaces along circular paths, backscattered periodically by the target, but also periodic echoes backscattered after *multiple internal reflections* of sound refracted into the shell.

The physical scattering interpretation allows us to formulate equations which relate the selected resonance characteristics to scatterer elastic properties, e.g., the shell outer and inner radii, shell material parameters and the inner fluid sound speed. These matching models are used by an automatic multi-hypothesis estimation method of resonance analysis designed to characterize a scatterer by its elastic properties. The water-filled shell data, acquired under roughly free-field conditions [1] and in the proud case were used to confirm the existence of assumed waves and to test the proposed method. For the proud case, the target scattering data used in this work, were recorded during an experiment performed by SACLANTCEN in April 1997, similar to that described in [5].

2

Sound scattering by a fluid-filled shell at broadside

Sound scattering investigations are focused on fluid-loaded thin-walled circular cylindrical shells filled with a generic fluid and insonified at broadside. In particular, the selection and study of a set of wave types backscattered by the examined class of objects are addressed. This study, carried out in the frequency domain, aims at associating the resonance frequencies detected in the scatterer form function with the selected types of waves, and, consequently, to understand how the resonance frequency characteristics change as the target elastic properties vary. The physical laws correlating measured resonance features with target properties are represented by means of analytical matching models applied in the data processing phase.

As shown in [14], from the comparison between RST and PPT applied to scattering by *empty/air*-filled cylindrical shells a good agreement was found in terms of phase speed dispersion curves of the scattered wave families. Here, following this approach, the theoretical investigations on fluid-loaded thin plane plates [13] are applied to fluid-loaded *liquid*-filled thin-walled shells. The plane-plate theory is preferred to RST although the current study is focused on circular shells. It allows one to derive more easily explicit, although approximated, analytical expressions of the phase speed of all the wave types observed both in plates and in shells in terms of all the target elastic parameters. The selected theory is limited to scattering by infinite targets insonified at broadside in the far field [11]. As an extension, next activities will concern also the study and analysis of sound scattering by finite targets as their aspect varies from broadside to endfire [15].

The free-field results are then adapted to the same targets when lying proud on a sea bottom. The main effects of interaction of the target with the sea bottom are predicted on the basis of the SSC model [5]. Those phenomena are selected that are expected to exist, and to follow approximately the same physical laws as in the free space case.

2.1 Problem definition

The physical interpretation of the resonance features one can outline in the response of a free-field fluid-filled thin-walled shell comes by analogy [14] from the study of plates of the same material and thickness loaded by the same fluids as the examined shell. Theory concerns scattering by thin solid plates (with shear speed c_s, compressional speed c_p, and density ρ, and thickness by either the same fluid [13][12] on both sides, or a different fluid [11][12] on each side. In turn, it consists of an extension of theory on scattering by plates either in vacuum [13][11] or fluid-loaded on one side only [11][2][8], respectively.

The plate-shell analogy is valid in the frequency range in which their thickness d remains smaller than the considered wavelength [8], i.e., under *thin-walled* conditions. Hence the solution of the equations formulated for the plate are approximately valid also for the corresponding shell.

2.2 Scattering by a fluid-loaded thin plate. Dispersion curves of surface waves

The analytical approach for tracking the steady-state waves propagating along a fluid-loaded plate considers the plate insonified by an incident plane wave as a two-dimensional wave-guide (see Fig. 1) in the xz plane. The behavior of the scattered waves can be studied from the solution of the characteristic equation for the vibration of the plate itself in terms of wave phase speed in the direction x along the plate axis as frequency varies [13][8]. For the general case of two different fluids with sound speeds c_i and densities ρ_i $(i = 1, 2)$ loading the plate on opposite sides, the steady-state wave-guide problem is defined in Appendix A and, assuming all the waves progressive, leads to the following characteristic equation [16]:

$$\sum_{i=1}^{2} (S_i \; A_i) - \frac{1}{\rho^2} \left(\frac{\rho_1}{k_{1,z}} - \frac{\rho_2}{k_{2,z}} \right)^2 k_s^8 \, k_{p,z}^2 = 0 \tag{2}$$

where

$$\begin{aligned} S_i = \; & 4k_{ph}^2 k_{s,z} k_{p,z} tanh\left(k_{p,z}\tfrac{d}{2}\right) tanh\left(k_{s,z}\tfrac{d}{2}\right) - \left(k_{s,z}^2 + k_{ph}^2\right)^2 tanh\left(k_{s,z}\tfrac{d}{2}\right) + \\ & -k_s^4 \tfrac{\rho_i k_{p,z}}{\rho k_{i,z}} tanh\left(k_{p,z}\tfrac{d}{2}\right) tanh\left(k_{s,z}\tfrac{d}{2}\right), \end{aligned} \tag{3}$$

and A_i derives from S_i by replacing $tanh$ with $coth$ everywhere. Further,

$$\begin{aligned} k_m &= \tfrac{2\pi f}{c_m}, \\ k_{m,z}^2 &= k_{ph}^2 - k_m^2 \end{aligned} \tag{4}$$

where $Re\{k_{m,z}\} > 0$, $m = 1, 2, p$ or s. The unknown parameter $k_{ph} = \frac{2\pi f}{c_{ph}}$ is the wave propagation constant in the direction x parallel to the plate, while the unknown

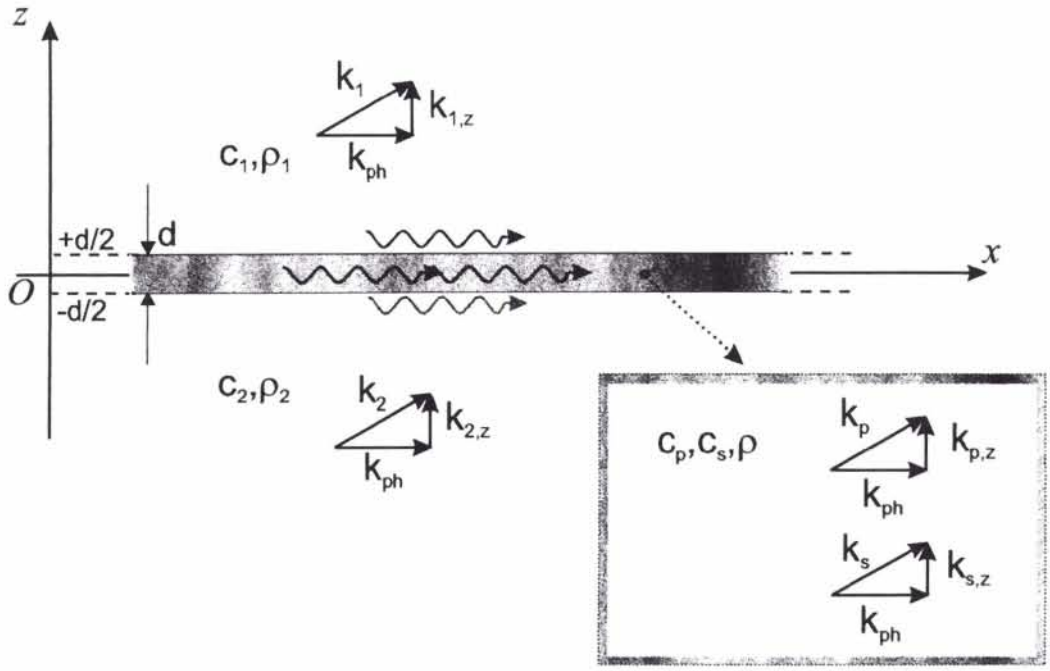

Figure 1 *Cross-section of a thin plane plate immersed into fluid 1 and fluid 2 at opposite sides.*

parameters $k_{m,z}$ $(m = 1, 2, p, s)$ are the wave number components in the direction z normal to the plate, as shown in the diagram of Fig. 1. Given the previous relations, the parameters $k_{m,z}$ are uniquely determined once k_{ph} is found.

In this work the solution of the characteristic equation is studied in the *fd* range (0,1) MHz mm, assuming the frequency f in the range (0,20) kHz and the thickness d in the range (0.005,0.05) m. Since the argument values of the transcendental functions are small (i.e., at most around unity), the hyperbolic sines and cosines can be replaced with good approximation by linear terms and unity, respectively, which simplifies the solution of (2). Under this approximation the equation is satisfied by a maximum of eight different solutions.

First the simpler case of one fluid loading both plate sides is analytically solved [13], then some hypotheses on the solution and interpretation of the more general case of two different fluids are proposed.

2.2.1 Plate loaded by the same fluid on both sides

If the fluids are identical on both sides, one can set $c_1 = c_2 = c_{fl}$, $\rho_1 = \rho_2 = \rho_{fl}$, $A_1 = A_2 = A$ and $S_1 = S_2 = S$. Hence, the characteristic equation (2) is reduced to

$$2SA = 0, \tag{5}$$

and, equivalently,

$$\begin{cases} S = 0 \\ A = 0. \end{cases} \tag{6}$$

Each equation of the system (6) is satisfied by four types of surface waves generating "symmetric" (S) and "asymmetric" (A) deformations with respect to the longitudinal axis of the plate. Two families are symmetric and the other two asymmetric.

The first symmetric wave family corresponds to the zero-order symmetric Lamb wave in vacuum, and hence is called the **zero-order symmetric Lamb-type wave** S_0 and its phase speed is:

$$c_{ph}^{S_0} = c_s \sqrt{4\left(1 - \frac{c_s^2}{c_p^2}\right)} \left[1 + \frac{j}{2} \frac{\rho_{fl}\, c_{fl}\, 2\pi f}{\rho c_s^2} \frac{d}{2} \left(\frac{1}{4\left(1 - c_s^2/c_p^2\right)} - \frac{c_s^2}{c_p^2} \right)\right]. \tag{7}$$

It corresponds to the compressional membrane wave type C introduced by the shell membrane wave theory [15]. Its imaginary part is small, and corresponds to a low attenuation due to radiation into the loading fluid, which increases with frequency in this frequency range and is null in the vacuum-loaded case, when the wave is also non-dispersive. Its real part corresponds to the characteristic speed c_* given by a combination of the shear and compressional speeds of the plate material,

$$c_* = c_s \sqrt{4\left(1 - \frac{c_s^2}{c_p^2}\right)}. \tag{8}$$

This parameter value is higher than that of the sound speed in water for most of solids, in particular for most of metals (see a list of c_* values for several solids in [4]). Consequently, the S_0 Lamb-type wave type is generally *supersonic*.

The second symmetric wave family appears only when the plate is fluid-loaded on both sides. It travels at the fluid-plate interface in the fluid (i.e., it is considered fluid-borne), and hence corresponds to the Scholte-Stoneley waves. It is called the **symmetric Scholte-Stoneley wave** S, and its phase speed dispersion curve expression follows:

$$c_{ph}^{S} = c_{fl} \left(1 - \frac{\left[\frac{\rho_{fl}\, c_{fl}\, 2\pi f}{\rho c_s^2} \frac{d}{2} \left(1 - \frac{c_{fl}^2}{c_p^2} \right) \right]^2}{32 \left[1 - \frac{1}{4} \frac{c_{fl}^2}{c_s^2} + \frac{c_s^2}{c_p^2} \right]} \right). \tag{9}$$

Having a purely-real-valued phase speed, this wave is not attenuated. As the term depending on frequency is much less than unity and slightly decreases with frequency, the wave is only slightly dispersive and always *subsonic*.

The first asymmetric wave family is the **zero-order asymmetric Lamb-type wave** A_0, which is a flexural surface wave traveling inside the plane plate. The phase speed is approximated at very low frequencies (i.e., for $fd \to 0$) by

$$c_{ph}^{A_0} = \sqrt[5]{\frac{4}{3}\left(1 - \frac{c_s^2}{c_p^2}\right)\frac{\rho}{\rho_{fl}}\left(\frac{d}{2}\right)^3}\,(2\pi f)^{\frac{3}{5}}\; e^{j\frac{4}{5}\frac{\pi}{2}} = Const\;(2\pi f)^{\frac{3}{5}}\; e^{j\frac{4}{5}\frac{\pi}{2}}, \qquad (10)$$

which has a small real part, and is therefore highly attenuated and difficult to distinguish in the scattering response in this frequency range. The modulus is identical to the phase speed of the fluid-borne **asymmetric Scholte-Stoneley wave** family A, which, having real phase speed, is not attenuated, and hides the A_0 wave resonances until they become supersonic [13][11], with

$$c_{ph}^{A} = Const\;(2\pi f)^{\frac{3}{5}}\,. \qquad (11)$$

As a consequence, at very low frequencies the A and A_0 waves resonances are positioned at approximately the same frequencies but with different phase speeds, which tend to coincide as the frequency increases until a "coincidence frequency", around which the A_0 wave from subsonic becomes supersonic. The two phase speed curves tend to deviate again at higher frequencies, as the A waves remain subsonic. The coincidence frequency varies with the loading fluid, the plate composition and thickness; for example, for a 6 mm thin steel plate in water, it occurs in the fd range (0.24, 0.3) MHzmm.

At high frequencies (as well as for thick plates), i.e., for $fd >> 1$ MHz mm, both Lamb-type waves are of Rayleigh type (i.e., the modulus of their phase speed tends to the plate material Rayleigh speed c_R), while the phase-speed modulus of both the symmetric and asymmetric Scholte-Stoneley waves asymptotically tends to the fluid sound speed c_{fl}, always remaining subsonic [13].

Figure 2 presents the dispersion curves of the Lamb-type and Scholte-Stoneley surface waves computed for a steel thin plate in water (d=6 mm, c_p = 5950m/s, c_s = 3240m/s, ρ = 7.7g/cm^3, c_{fl}=1521 m/s, ρ_{fl}=1 g/cm^3).

The other four of the eight solutions of the system Eq. (6) have negative attenuation, which means that they have negative group speed, i.e., travel in the opposite direction ($-x$) with respect to the considered waves [13].

At higher fd values, the approximated asymptotic solution of the characteristic equation system Eq. (6) has been provided by [13]. Although beyond the scope of the

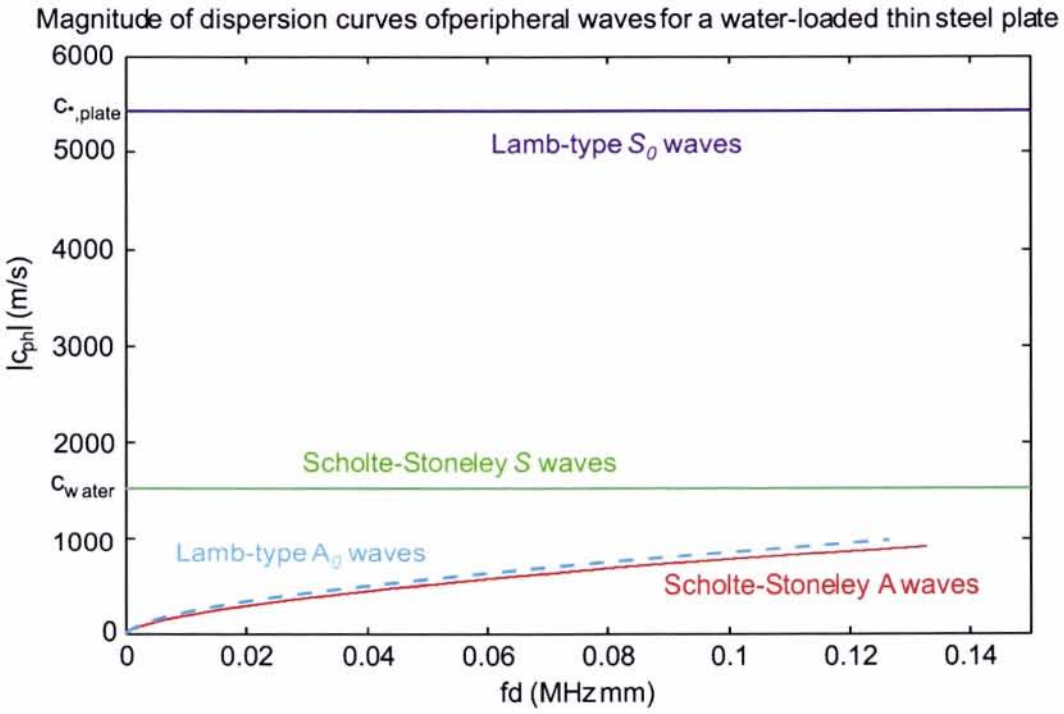

Figure 2 *Predicted dispersion curves of the main surface wave families traveling on a water-loaded thin steel plane plate (d=6 mm).*

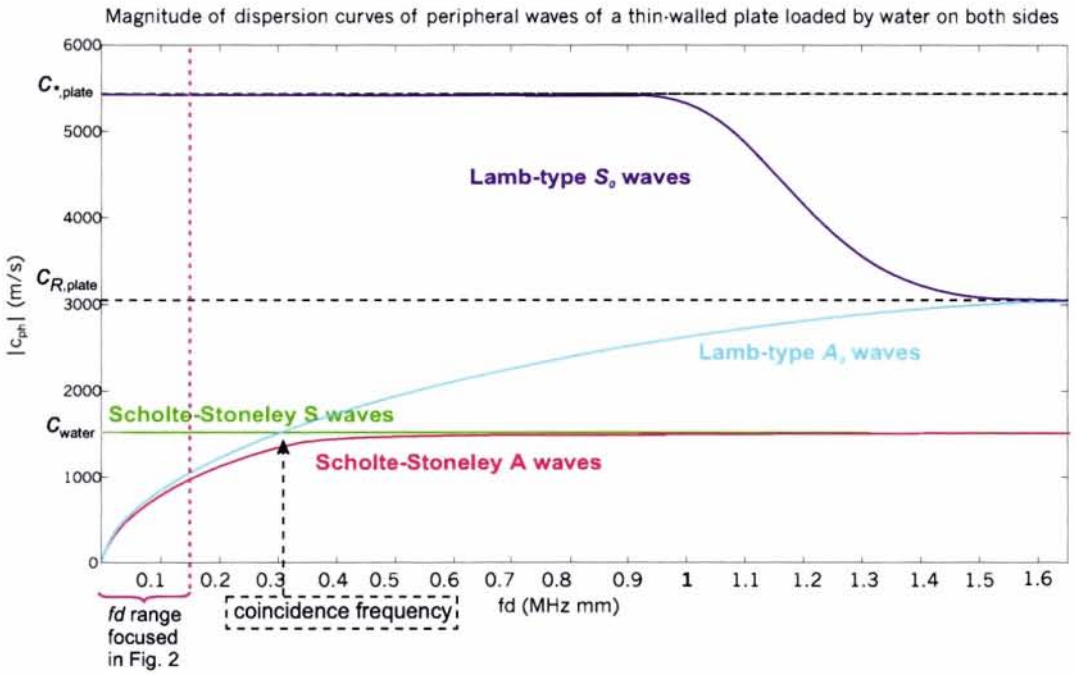

Figure 3 *Sketch of phase dispersion curves of a thin plate loaded by the same fluid* fl *on both sides (study from low to high frequencies).*

present report, Fig. 3 illustrates the global behavior of the phase speed dispersion curves, for every peripheral wave generated at low frequencies. At intermediate frequencies the curves are sketched for connecting low and high frequency branches.

The plot shows the predicted behavior of A, S, A_0, and S_0 waves. The dispersion curves related to the A_0 and A waves are approximated but clearly show wave coupling and reciprocal deviation (also called *repulsion* [16]) at intermediate frequencies when both approach the fluid sound speed and the A_0 wave becomes supersonic (i.e., around the coincidence frequency).

2.2.2 *Plate loaded by two different fluids*

When fluid 1 is different from fluid 2, the solution of Eq. (2) is not provided analytically. Qualitative considerations are outlined and hypotheses are introduced which are partially confirmed by the literature [11][12]. In Fig. 4, hypothetical phase speed dispersion curves are proposed. Without loss of generality it is assumed $c_1 < c_2$.

The considerations which have led to this plot start from the comparison of the previously examined plate with the case of an identical plate air-loaded at one side and water-loaded at the other [2][8]. The behavior of fluid-borne A waves in terms

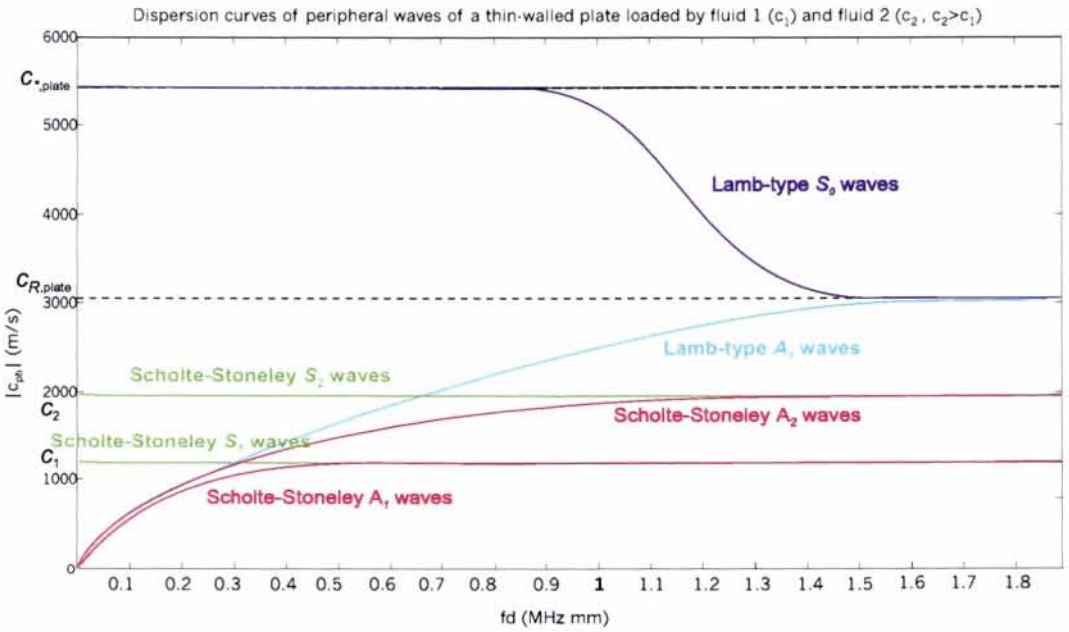

Figure 4 *Sketch of assumed phase dispersion curves of a thin plate loaded by fluid 1 and fluid 2 on opposite sides (study from low to high frequencies).*

of the dispersion curve is not significantly changed when water is replaced by air (or vacuum) at one side.

The plate-borne S_0 waves are similar in both cases. In particular, the real part of the phase speed is largely unchanged, while the imaginary part, related to wave radiation into the loading fluids, is expected to depend on the impedance of both fluids. In particular, the wave attenuation in the air-filled case has been calculated at half the attenuation computed when the plate is loaded by the same fluid on both sides [14]. However, as the attenuation of S_0 Lamb-type waves is low for any loading fluid, the phase speed is considered unaffected by the properties of the outer medium. More precisely, even when attenuation, in this case due to the loading fluid, affects only slightly the wave resonance frequencies, it plays an important role in terms of *damping effect*. The wave energy becomes progressively weaker with each periodic backscatter, with consequences in the data processing methodology of resonance frequency extraction, described in Section 3.

The S wave family is generated only if the plate is fluid-loaded on both sides, hence it depends on both fluids, but its properties are assumed to be more strongly influenced by the properties of the fluid in which it travels.

For symmetry, one S_l and one A_l Scholte-Stoneley wave family (l=1,2) are expected to travel on each of the two fluid-plate interfaces. The dispersion curves are assumed

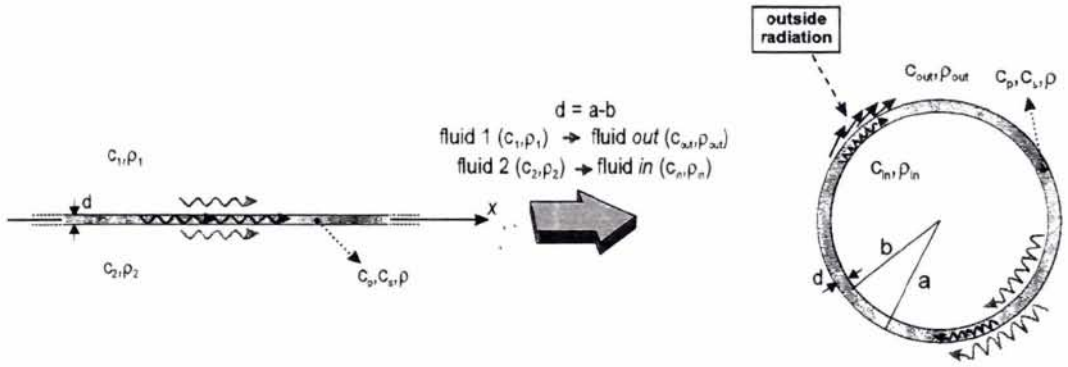

Figure 5 *Extension from a plate to a shell with the same thickness and elastic characteristics.*

to be affected primarily by the properties of the fluid in which they travel.

Coupling between the A_0 Lamb-type wave and the asymmetric Scholte-Stoneley waves A_1 and A_2 is predicted for analogy with the case of single-fluid loading: a "repulsion" phenomenon between the A_0 and each of the two asymmetric Scholte-Stoneley wave dispersion curves is forecast, whenever the sound speed of one of the two loading fluids is reached.

2.3 Extension to shells. Resonance feature selection and matching models

Provided the analytical expression of the surface wave dispersion curves in the case of a thin plane plate, the study is extended to circular shells, in order to verify the applicability of the equations and to complete the analysis with a ray-theory-based description of those phenomena, peculiar to liquid-filled, thin-walled circular shells.

If the plate is replaced with a circular, cylindrical shell with outer radius a, inner radius b, the same thickness d, which now corresponds to $(a - b)$, and the same elastic parameters (see Fig. 5, where fluid 1 is called fluid *out* and fluid 2 is called fluid *in*), the types of waves introduced so far have been proved to be generated and to maintain roughly the same properties [8][11][12]. However, the attenuation of each backscattered wave generally increases because of the object curvature, which causes the radiation into the surrounding fluids to increase. Hence, the related phase speed dispersion curves are expected to deviate slightly from those predicted. As the deviation has been evaluated to be small [14], the results obtained in the previous subsections remain valid. Figure 6 lists on the left a set of classes of surface waves which can be backscattered by thin-walled shells with circular cross-section. In the first class of waves (i.e., the shell borne waves) the symmetric and asymmetric Lamb-type waves are included.

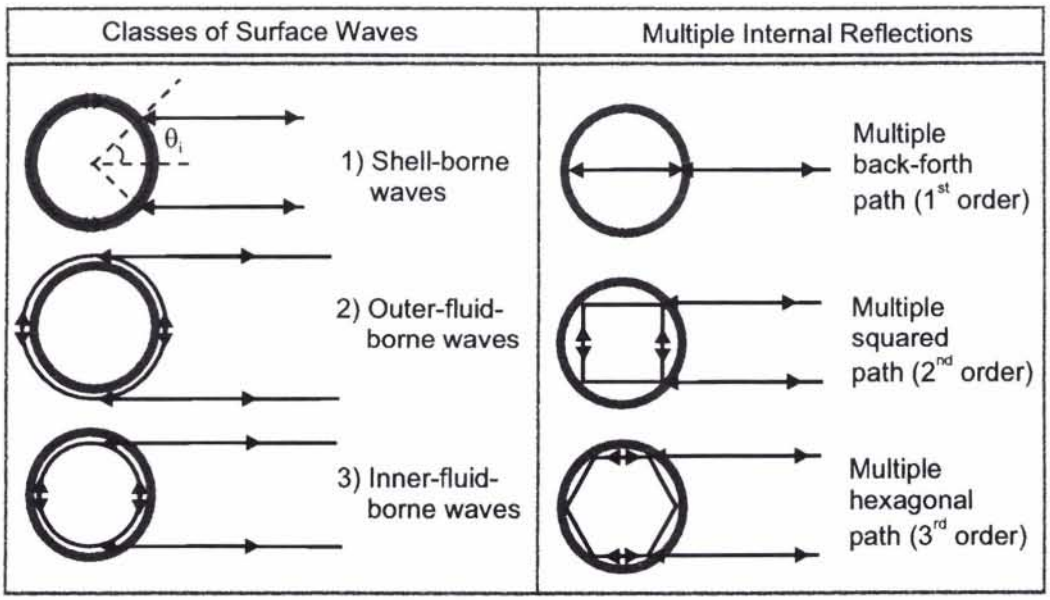

Figure 6 *Simplified travel paths of classes of surface waves (left) and internal multiple reflections (right) backscattered by a thin-walled, fluid-filled circular shell in the free field.*

Under thin-walled conditions, part of the sound is assumed to be transmitted through the shell, propagated into the inner fluid and reflected several times, before being partially backscattered externally [12]. The sound component remaining inside is expected to continue traveling on the same paths, giving rise to periodic backscattered waves. The internal paths of transmitted waves must be either the direct path or regular polygons of even order (i.e., of 4, 6, etc. sides) in order to generate backscattered waves (Fig. 6). This phenomenon is significant when the inner fluid is a liquid. As energy decreases as their order increases, only the first 3 orders (i.e., the internal direct, squared and hexagonal paths) are considered.

If a plane wavefront insonifies the target at broadside, pairs of waves of the same kind, generated at angles of incidence symmetrical with the axis source-target, traveling in opposite directions, contribute coherently to sound backscattering. This is shown in Fig. 6 by double arrows along the travel paths.

The analytical formalization of wave variations with frequency allows the construction of models of relationships between resonance characteristics and target elastic properties. For surface waves, using the predicted formulas of the wave dispersion curves proposed above, one can predict the value of the n^{th}-order resonance frequency f_n^W of the surface wave family W by applying the equation

$$f_n^W = n \frac{\left| c_{ph}^W \right|}{2\pi R}, \tag{12}$$

where R is either the outer or the inner radius of the shell depending on whether the wave travels at the outer or inner shell interface. This leads to the discretization of wave phase speed corresponding to resonance modes.

From the phase speed dispersion curve of a wave W, the corresponding group speed c_g^W is derived as [17]

$$c_g^W \approx |c_{ph}^W| + f \frac{\delta |c_{ph}^W|}{\delta f}. \tag{13}$$

Equation (13) assumes that the relative variation between the phase speed modulus of two successive resonances is small, i.e., that $\delta |c_{ph}| \ll 1$. The group speed of the mode f_n^W can be defined by the approximation

$$c_{g,n}^W = 2\pi R \, \Delta f_{(n+1),n}^W, \tag{14}$$

where $\Delta f_{(n+1),n}^W = f_{n+1}^W - f_n^W$. Equations (12) and (14) depend on the resonance modal order n. For non-dispersive and almost-non-dispersive waves, having at least roughly constant group speed,

$$c_g^W = 2\pi R \, \Delta f^W, \tag{15}$$

where Δf^W is the mean frequency distance between two successive resonances of the W family, implying the presence of (roughly) equally-spaced, adjacent resonance frequencies.

For localizing the "resonance frequencies" of the periodic, multiple internal reflections, namely r_l where l is the wave family order (l=1,2,..), general formulae can be introduced. They are approximated by assuming the waves are non dispersive, i.e., with roughly constant distance Δf^{r_l}, and travel inside the shell at the speed of sound in the inner fluid, c_{in}. Hence the wave resonance frequencies are expected to follow the ray theory:

$$f_n^{r_l} = n \frac{c_{in}}{P_{2l}}, \tag{16}$$

$$\Delta f^{r_l} = \frac{c_{in}}{P_{2l}}, \tag{17}$$

where P_{2l} is the length of the internal back-forth direct path for $l = 1$ and the length of the perimeter of the inscripted polygon of $2l$ sides for $l > 1$:

$$P_l = 4l \, sin\left(\frac{\pi}{2\,l}\right) \, b, \tag{18}$$

In this approximation, the resonance characteristics depend only on the inner fluid sound speed and shell inner radius.

2.3.1 Shell-borne peripheral waves: Lamb-type wave families

From the solution of Eq. (2) and comparison with RST-based results (e.g., compare [13] with [2]), it has been proven [14] that the symmetric and asymmetric Lamb-type wave families generated by thin-walled, air-filled or empty shells also exist when the same object is filled with a liquid.

As the A_0 Lamb-type waves are coupled with the fluid-borne asymmetric Scholte-Stoneley waves [8][12], their dispersion curve is expected to be affected by fluid-loading. However, at very low frequencies (i.e., for $fd \ll 1$ MHz mm) they are usually so highly attenuated that their resonance frequencies can not be extracted as features from a measured target response.

The S_0 wave characteristics have been analytically demonstrated in [14] to be affected very little by fluid-loading. In particular, if compared with the empty/air-filled shell case, their resonance frequencies are slightly shifted in location of an almost constant quantity, depending on the inner fluid properties. The frequency shift is due to the radiation of the wave into the inner fluid (if liquid). For liquid-filled shells most of the S_0 modes, which correspond to marked and equidistant dips in the spectral response of an empty or air-filled shell, interfere with other waves, the resonance frequencies of which occur at the same local ranges. Hence, they are frequently partially concealed by stronger phenomena.

Thanks to the good agreement between PPT and RST, the resonance localization of the S_0 Lamb-type wave resonances of the circular shell are analytically provided by PPT. They are presented only for the simpler case of two identical loading fluids. If the two fluids are similar in terms of impedance, the analytical models are expected to be approximately valid. The resonance location of the n^{th} mode $f_n^{S_0}$ can be computed from Eq. (7) by replacing f with $f_n^{S_0}$ and $c_{ph}^{S_0}$ with $f_n^{S_0}\, 2\pi a$ (according to Eq. (12)):

$$f_n^{S_0} = \frac{1}{\frac{2\pi a}{n\, c_*}\sqrt{1 - n^2\, c_*^2\, \frac{1}{4} c_*^2 \left(\frac{\rho_{fl}\, c_{fl}}{\rho\, c_*}\right)^2 \left(\frac{h}{2}\right)^2 \left(\frac{1}{c_*^2} - \frac{1}{c_p^2}\right)^2}}. \tag{19}$$

For most solids with $c_p \approx c_*$, and sufficiently small dimensionless shell thickness $h = \left(\frac{d}{a}\right)$ and relative impedance fluid-shell, the second term under the square root is much smaller than unity until n is of the order of hundreds. Hence Eq. (19) can be approximated with:

$$f_n^{S_0} \approx n \frac{c_*}{2\pi\, a}, \tag{20}$$

giving

$$\Delta f^{S_0} \approx \frac{c_*}{2\pi\, a}. \tag{21}$$

In this case the adjacent resonance distance becomes roughly constant and depends only on the outer radius and shell material shear and compressional speeds.

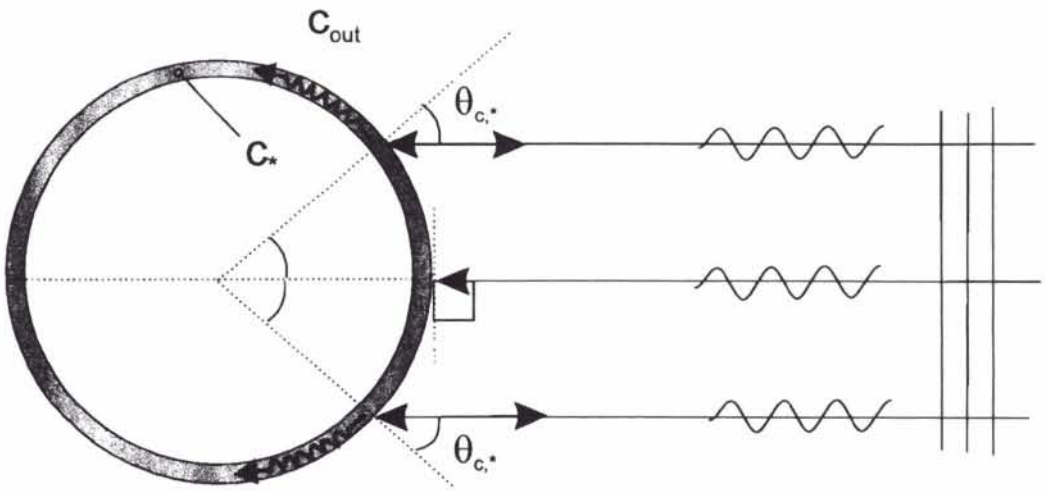

Figure 7 *Geometry of generation and backscattering of the S_0 Lamb-type waves.*

These waves are assumed to be generated by sound insonifying the shell surface at an average angle (with the normal to the interface)

$$\theta_i^{S_0} = \theta_{c,*}, \tag{22}$$

where $\theta_{c,*}$ is the shell critical angle relative to its characteristic speed c_* and therefore, defined as:

$$\theta_{c,*} = asin\frac{c_{out}}{c_*}. \tag{23}$$

Figure 7 shows the related geometry.

In conclusion, although more difficult to detect, the resonances of this family follow approximately the same laws presented in [4] for fluid-loaded, empty or air-filled shells.

2.3.2 *Fluid-borne peripheral waves: inner and outer Scholte-Stoneley waves*

The analytical solution for inner and outer Scholte-Stoneley waves is limited to the case of the same fluid inside and outside the shell. If the two fluids are different an approximated extension is proposed.

As a consequence of Eq. (12), the extension from plate to shell, allows one to assume that the fluid-borne wave families generated in the case of plates fluid-loaded on both sides, are divided into two sub-families, one for each shell side. For example, from the symmetric Scholte-Stoneley family S predicted in the plate case, two analogous families with coinciding phase speed c_{ph}^S (similar to that of the plate S wave) should

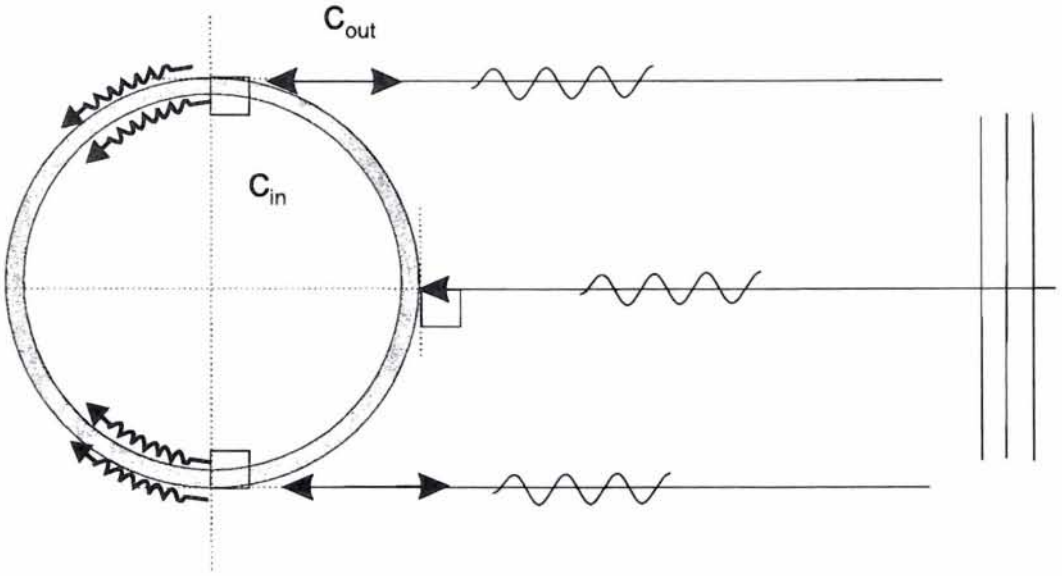

Figure 8 *Geometry of generation and backscattering of Scholte-Stoneley waves.*

be generated, one traveling in the outer and one in the inner fluid at the two shell interfaces. The same phenomenon should be expected of A waves.

These waves are assumed to be excited on average where the direction of the incoming wave is approximately perpendicular to the normal vector of the cylinder cross-section [8], i.e., around the top and bottom of the cylinder assuming an incident wave traveling from right to left (see Fig. 8). In the following this will be referred to as *tangential incidence.*

Following different, although close, circular paths, they are expected to have resonance modes of the same order located at different frequencies:

$$f_n^{m_{in}} = n \frac{\left|c_{ph}^m\right|}{2\pi\, b} \tag{24}$$

$$f_n^{m_{out}} = n \frac{\left|c_{ph}^m\right|}{2\pi\, a} \tag{25}$$

with $m = A, S$.

The S waves have been predicted by PPT to be unattenuated and only slightly dispersive. Dispersion increases with frequency in this range. For fixed frequency, it increases with shell thickness. If the inner and outer fluids have the same properties (i.e., $c_{in} = c_{out} = c_{fl}$ and $\rho_{in} = \rho_{out} = \rho_{fl}$), the group and phase speeds of the inner and outer S waves tend to, but remain less than the fluid sound speed c_{fl}.

The resonance frequency locations can be computed by replacing the phase speed expression of Eq. (9) in Eqs. (24) and (25) with $m = S$.

In the general case of different fluids, the group and phase speeds of the inner and outer symmetric families are assumed to tend towards the inner and outer fluid sound speed c_{in} and c_{out} respectively (see the reference plate case in Fig. 4). Under these assumptions, the S_{out} resonance mode locations can be thought to depend only on the outer fluid speed and shell outer radius,

$$f_n^{S_{out}} \approx n\frac{c_{out}}{2\pi a}, \tag{26}$$

and the inner wave resonance locations on the inner fluid speed and inner radius:

$$f_n^{S_{in}} \approx n\frac{c_{in}}{2\pi b}. \tag{27}$$

From a geometrical point of view the inner S waves can be perceived as an unattenuated internal transmission/reflection wave of infinite order, i.e., with polygonal number of sides $2l = \infty$, namely r_∞. The A_{in} and A_{out} frequency modes can be derived from Eq. (11) in the case of identical fluid inside and outside,

$$f_n^{A_m} \approx n\frac{c_*}{2\pi R}\sqrt{n^3\frac{1}{3}\frac{\rho}{\rho_{fl}}\left(\frac{d}{2R}\right)^3}, \tag{28}$$

where $R = b$, $m = in$ for the inner family, and $R = a$, $m = out$ for the outer family. However the formula above is valid only at very low frequencies (i.e., for $fd \ll 1$ MHz mm).

In subsection 2.2.2 the phase speed characteristics of the A waves traveling at one side of a plate have been assumed to be influenced little by the fluid at the other side. Hence, in the shell case, it is assumed reasonable to consider Eq. (28) to be approximately valid for A_{in} and A_{out} waves in the generalized situation of two different fluids.

2.4 *Interpretation of the scatterer response in terms of selected acoustic phenomena*

The validity of the scattering interpretation based on PPT and ray theory is verified by fitting the solution of the equations proposed in the previous subsection with RST-based predictions of acoustic scattering by a circular, thin-walled shell.

The detection and identification of the expected acoustic scattering phenomena in the frequency domain in terms of related wave resonances is presented with reference to simulated data obtained from a RST-based model [3]. The simulator provides the

scatterer complex Transfer Function (TF) $H(f)$, defined as the ratio of the scattered and the incident pressures, p_s and p_i respectively, in the frequency domain:

$$H(f) = \frac{p_s}{p_i}. \tag{29}$$

The analysis is performed on the TF spectrum, normalized by its maximum value. In the study of simulated data, a target is taken as a reference and for each set of simulations, only one parameter is changed in a certain range.

The reference canonical target is an infinite, steel, circular, cylindrical shell, submerged in water, filled with water and insonified at broadside. Its response is studied in the frequency range (0,25) kHz. The nominal water parameters are sound speed $c_{fl} = 1521\text{m/s}$ and density $\rho_{fl} = 1\text{g/cm}^3$. The inner and outer fluids are assumed to be identical. The reference outer radius a is 25 cm, and the reference inner radius b is 24.4 cm. As $h = 0.024$, the shell is very thin in the frequency range considered, as established in Table 2.3 of [4].

Figure 9 shows the scatterer TF spectrum model as its inner radius (top) and outer radius (bottom) vary.

The bottom row of the upper image coincides with the top row of the lower image, in order to provide one common reference, which is the simulated spectral response of the target having $a = 25\text{cm}$ and $b = 24.4\text{cm}$. The analysis of these simulations allows us to associate the main resonance features with the predicted scattering phenomena the physical laws of which were analytically formulated in subsection 2.3.

If a 25 cm radius shell in sea water is considered, the frequency range (0,30) kHz corresponds to the ka range (0,30.98). In the real case studies that will be presented in this report, the frequency range of interest will be about (2,20) kHz, i.e., (1.03,20.65) ka. In the selected range, for the sake of clarity the proposed simulation plots present only some examples of wave resonance identification.

In the upper plot, all the wave families whose resonance frequencies are inversely proportional to thickness are evident (i.e., r_l with l=1,2,3, and S_{in} wave types) and can be seen to follow hyperbolic curves. Some S_0 Lamb-type wave resonances can be identified, located along almost vertical lines. The outer Scholte-Stonely waves A_{out} follow quasi parabolic curves changing with frequency, which are again very evident in the lower plot following another family of parabolic curves. This is in agreement with Eq. 28 where the A_{out} resonance modes are shown to depend on the inner and outer radii through shell thickness d. In this frequency range, their resonance locations increase strongly with thickness, for fixed modal order (see Eq. (28)). In particular, they can be distinguished only for thick and quasi-thick (i.e., for $h > 6$ %) shells. In addition, the energy enhancement corresponding to the strong-bending region which characterizes the scattering spectrum of air-filled (or empty) thin shells

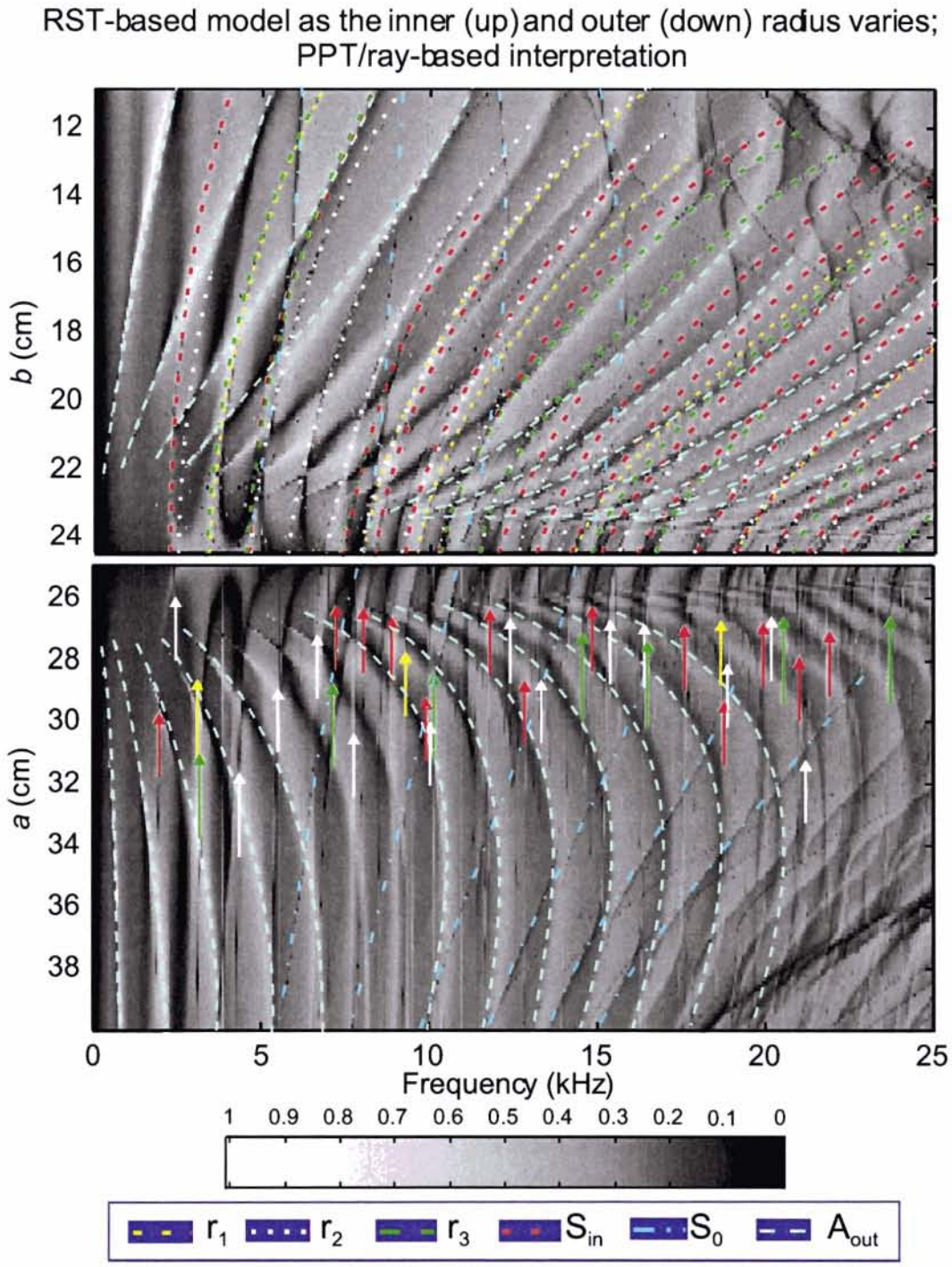

Figure 9 *Scattering model (linear scale) of a steel water-loaded water-filled shell at broadside. Top: simulations as shell inner radius b varies (*$b \in [9 : 0.1 : 24.9]$ cm, $a =$ 25cm*). Bottom: simulations as shell outer radius a varies (*$a \in [24.5 : 0.1 : 32]$cm, b=*24.4* cm*).*

cannot be observed here. This makes the extraction and identification of the A_{out} resonances more difficult. Consequently, this wave family is not selected as a feature useful for the characterization of thin-walled shells.

In the lower plot the most evident wave families are the inner-fluid-borne ones, the resonance locations of which depend only on the inner radius and inner fluid and are constant as the outer radius varies, given a modal order (i.e., they are on almost straight vertical lines). This shows that the proposed approximated formulas (16) and (27), which neglect dependence on the other geometrical and geophysical parameters, are consistent with the selected model.

Finally, for the sake of completeness, we add that the hyperbolic curves which can be seen in the top-right corner of the upper image and in the bottom-right corner of the lower image correspond to modes of Transverse Whispering Gallery waves of different orders, which are backscattered when the cylindrical target is solid or thick-walled shell [2].

As the Scholte-Stoneley S_{out} wave family can be distinguished only in the case of very thin shells, Figure 10 presents a zoom of the previous images for $d \in [6, 25]$ mm. Some S_{out} resonance modes are identified: in the upper plot their locations follow vertical straight lines as the inner radius varies, in the lower plot they follow hyperbolic curves as the outer radius varies, in accordance with the theoretical predictions in Section 2.3 (see Eq. 26).

Note that no A_{in} wave resonance has been identified on the simulated data of Figs 9 and 10. Hence this family will be not used as a feature for the target parameter estimation.

In conclusion, these simulation results confirm the consistency between the analytical formulation of the physical laws and the RST-based scattering model, and show how the selected wave types are expected to appear in terms of sharpness and energy level in the free-field TF model.

2.5 *Resonance interpretation of the proud target model*

It is assumed that the target on a flat sediment bottom is insonified with grazing angle θ_g. This hypothesis introduces a boundary in the previous free-space problem (Fig. 11). The bottom geophysical properties are compressional sound speed c_3 ($c_3 > c_{out}$) and density ρ_3. Assuming $c_3 > c_{out}$ is reasonable for sediments that would support a proud object.

Two main components of sound are assumed to insonify the target according to the *single-scattering model* proposed in [5].

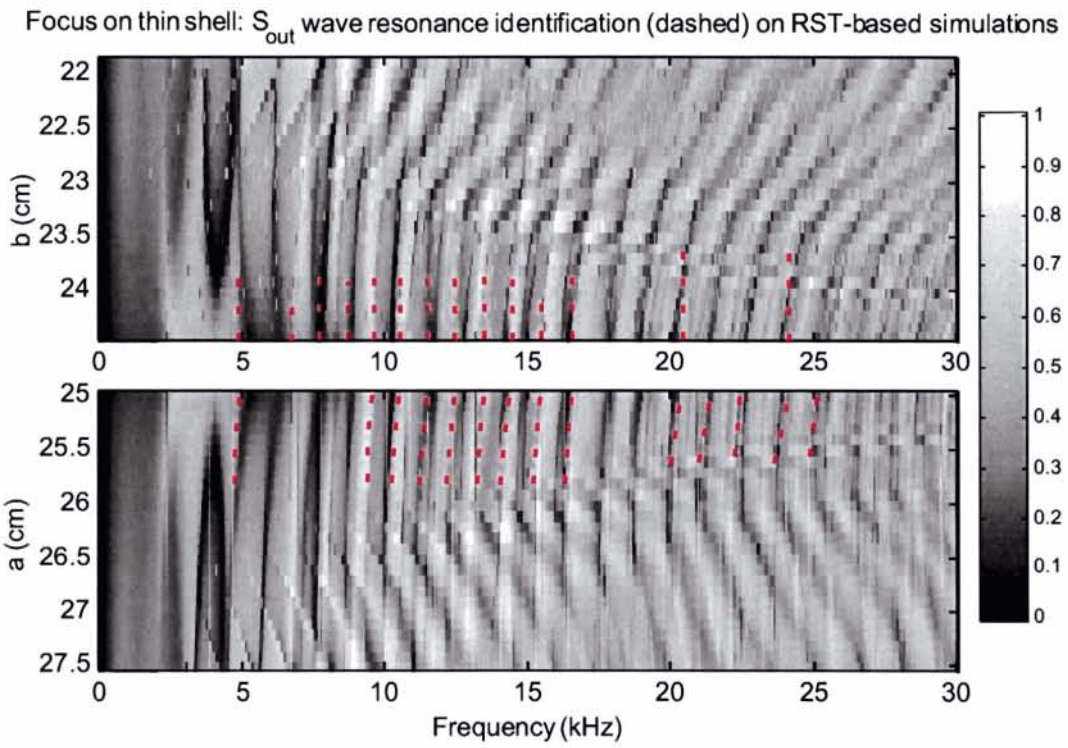

Figure 10 *Scattering model (linear scale) of a steel water-loaded water-filled shell at broadside. Up: simulations as shell inner radius b varies (*$b \in [9 : 0.1 : 24.9]$ cm, $a = 25$cm*). Down: simulations as shell outer radius a varies (*$a \in [24.5 : 0.1 : 32]$cm, b=24.4 cm*).*

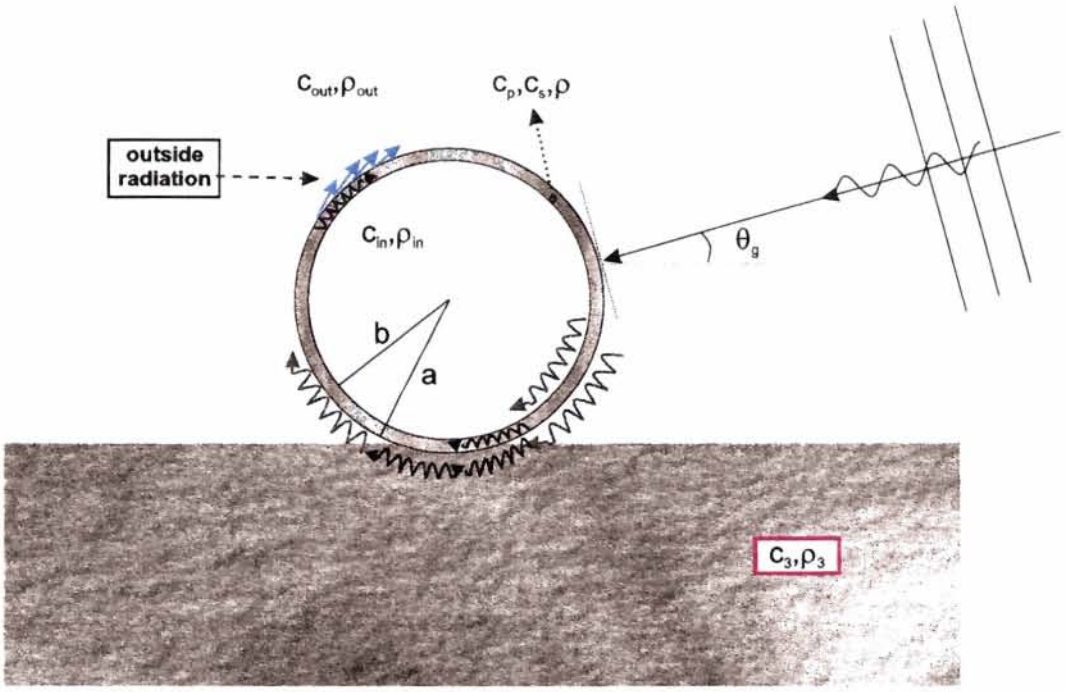

Figure 11 *Geometry of the scattering problem when the cylindrical shell lying on a flat bottom halfspace is insonified at broadside at the grazing angle* θ_g.

Wave component following the direct path
The first main component of the incident wave consists of the sound following a direct path between the transmitter and the target. This is expected to give rise to phenomena similar to those presented in the free-space case. Figure 12 sketches the behavior of the same classes of waves which have been selected in the free-field case and are supposed to be generated by the direct sound wavefront in the present geometry. The influence of the sea bottom boundary is outlined.

The *shell-borne* surface wave types generated by this incident sound wavefront are expected to be present with characteristics very similar to those described in the free-field case, as they are generated and backscattered at an average angle ($\theta_{c,*}$) which is usually far from the bottom boundary (see Fig. 12.(a)). Hence the wave generation and radiation phenomena are not expected to be influenced by the boundary. This class of waves is characterized by a certain radiation into the surrounding medium, implying radiation into the sediment when they travel along the shell-sediment interface. This should cause higher attenuation than in the free-field case (owing to the lower relative impedance between the shell and the sediment) and, as a consequence, a shift of resonance locations towards higher frequencies. However, the path along the shell-sediment interface is a relatively small fraction of the circular path followed by the waves, hence the resonance frequency shift is not expected to be

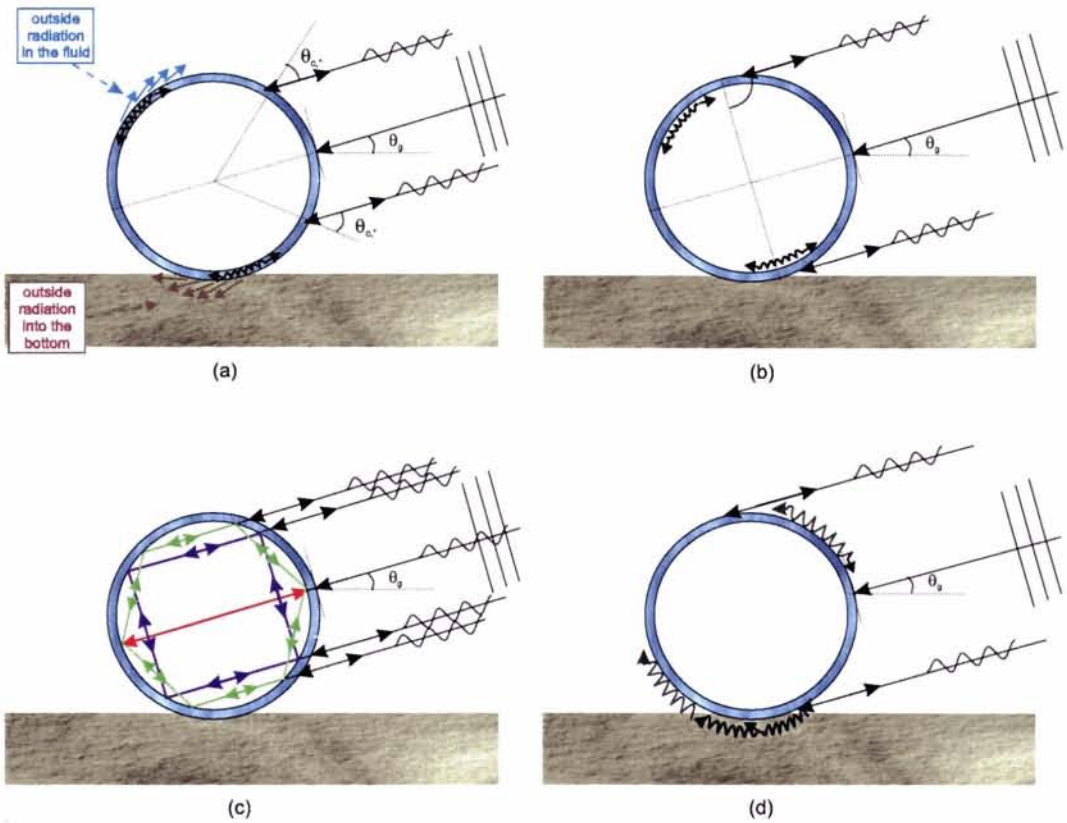

Figure 12 *Simplified scheme of travel paths of the main periodical wave families backscattered by a fluid-filled thin-walled shell lying proud on a bottom (direct path).*

significant and the shell-borne wave dispersion curves presented for the free space case remain applicable.

The generation of *inner-fluid-borne* surface wave families is caused by tangential incidence and backscattering which can be significantly affected by the presence of the seabed boundary only if the target is partially buried into the sediments and the grazing angle is low. In this case, this class of waves, if existing, is partially generated and backscattered where the target surface is in contact with the sediment and hence could have significantly different characteristics in terms of phase speed and backscattered energy level. Otherwise (see Fig. 12.(b)), they should maintain the same properties as in the free space and follow the same physical laws, as their phase speed is assumed to be weakly affected by the outer medium.

Also, the wave types derived from *internal transmission/reflections* of the first orders should be weakly affected by the bottom boundary, as they are generated and backscattered at average angles (i.e., 0°, 45°, 60°, etc.), far enough from the boundary (see Fig. 12.(c)) that they cannot be significantly affected.

The *outer-fluid-borne* class of waves is expected to be influenced by the presence of the sea bottom because it travels at the shell outer interface in the outer medium and is generated and backscattered tangentially (see Fig. 12.(d)). For their tangential generation and backscattering, the same considerations referred to inner-fluid surface waves can be applied, hence the presence of the boundary should still allow their existence. With regard to their travel path, they are still expected to propagate from the fluid through the sediments again to the fluid along the shell interface, but with a change of phase speed according to the geophysical properties of the medium in which they travel. In any case, as the path through the sediments is small with respect to the global path (as occurs if the target is not partially buried), the characteristics of the wave phase speed along a complete circular path should not deviate significantly from that predicted in free-space. For this reason, the outer-fluid-borne waves are still predicted to follow the equations introduced above for the free-field case.

Wave component following a multi-path (one reflection on the bottom)
According to the SSC model, the second main component of the incident wave is reflected by the seabed in front of the target, before hitting the target, in flat bottom conditions by comparison with the incident sound wavelength (Fig. 13) [5]. In this case, the bottom would behave as a *mirror* and a *virtual image* of the target cross-section would be generated. If the grazing angle is below the sediment critical angle and the bottom is flat enough, a part of this wavefront is expected to propagate through the bottom as evanescent waves [18], otherwise a part is expected to penetrate into the bottom sediments, according to Snell's law. Determining which phenomenon among reflection and refraction dominates is a complicated problem involving many variables, such as frequency, grazing angle and bottom geophysical

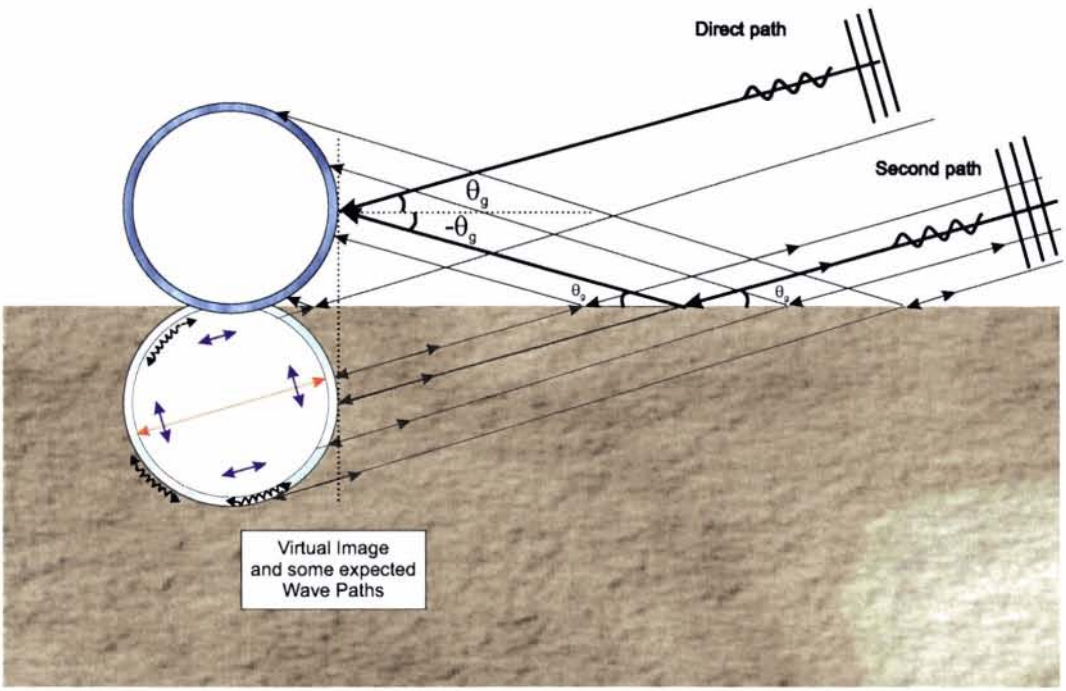

Figure 13 *Geometry of the* single scattering approximation. *Focus on the bottom-interacting sound components ("mirror" effect of the bottom).*

characteristics (e.g., homogeneity, porosity, grain size, etc.) and flatness in terms of wavelength [19].

Also, each of these two incident wavefronts can cause the target to scatter back the sound through various paths, either direct or bottom-reflected.

In general, all the sound wavefronts impinging on the target are expected to generate resonance phenomena as assumed above for the direct sound component. This can be clarified by the comparison of Fig. 12 with Fig. 13, the latter showing the paths of some of the wave types assumed to be generated by the reflected wavefront, to travel around and through the target and to be periodically backscattered along the same path followed by the incident reflected wavefront. As a consequence, one could predict the same periodicities of all generated waves belonging to the same family and hence, the same frequency locations of the corresponding resonance modes. However, interference among waves of the same family, generated by different wavefronts, is expected in terms of their phase and amplitude as the frequency varies, given a certain fixed grazing angle.

The target global TF $H(f)$ would change with respect to that obtained by the direct wavefront only, namely $H^d(f)$. The TF can be thought of as the linear superposition of N response contributions, each following a different path. If the hypotheses of plane wave and flat bottom are assumed, by extending the SSC model [5] (Eq. (3)) each response contribution i can be represented as

$$H^d(f)\ R_i(\theta_g)\ e^{j2\pi f \tau_i(\theta_g)}, \tag{30}$$

where $\tau_i(\theta_g)$ is the time delay with respect to the direct wave component and $R_i(\theta_g)$ is the reflection coefficient of the bottom. Figure 14 shows how $\tau_i(\theta_g)$ is obtained, known θ_g, for the case of one bottom bounce. If the compressional wave attenuation in the sediment is non-zero, $R_i(\theta_g)$ is complex, and has amplitude close to unity if the grazing angle is less than the bottom critical angle θ_c [18][20]. Hence, the target TF can be expressed as

$$\begin{aligned} H(f) &= H^d(f)\left[\sum_{i=0}^{N}\left(e^{j2\pi f\tau_i(\theta_g)}R_i(\theta_g)\right)\right] \\ &= H^d(f)M(f,\theta_g), \end{aligned} \tag{31}$$

where the 0-order element of the summation corresponds to the direct response, hence $R_0(\theta_g) = 1$ and $\tau_0(\theta_g) = 0$. It consists of the direct contribution $H^d(f)$ modulated in frequency by the complex function $M(f,\theta_g)$ which, for each frequency f, causes a change of amplitude and phase of the direct TF contribution.

If this effect is related to the TF resonance frequencies detected in the TF spectral domain as dips, peaks, or dip-peak pairs, modulation is expected not to cause frequency shift with respect to the direct response, hence not to affect the frequency

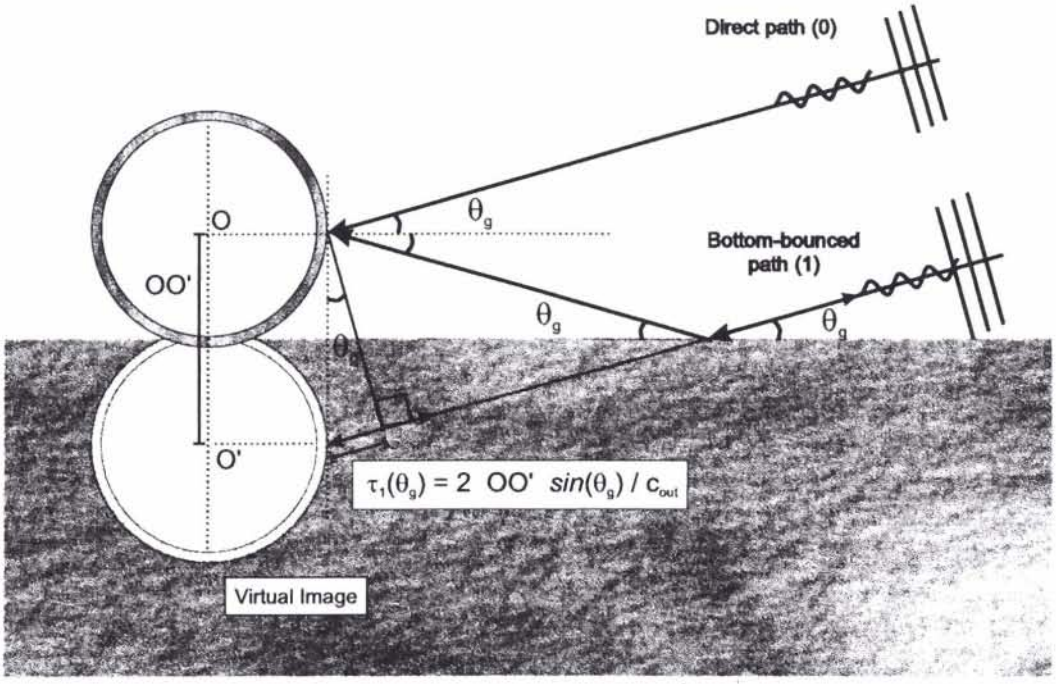

Figure 14 *Time delay between the direct and the bottom-bounced paths.*

location of the resonance modes of any expected periodical wave family. This confirms the considerations on the physical characteristics of periodical waves of the same kind generated by the different wavefronts. If the analytical laws describing the scattered wave resonance variations according to target parameters, studied for the free-space case, are considered valid for the proud-target direct scattering contribution, the same is applicable to the analysis of the proud target global response, including multi-path contributions.

However, at certain frequencies the modulation effect might cause an evident change of the TF spectral amplitude with the consequent partial or complete cancellation of the resonance modes located at those particular frequencies. A broadband approach based on the TF spectral analysis on a relatively wide band is therefore necessary in order to collect a sufficient subset of resonance frequencies belonging to each periodical wave family selected, even when some are not detectable because of disruptive interferences.

Although the theoretical interpretation is based on the hypothesis of incident plane wave, the existence and power of the multi-path scattering contributions depend also on the beampatterns of transmitter and receiver (for a fixed grazing angle).

Other parameters are involved in the backscattering mechanism. The influence of the bottom on resonance scattering (direct and multi-path) and in particular on the

Wave Family	Related Parameters	Application	Reference
S_0 Lamb-type	c_*, a	Free-field & Proud	Eq. (20)
S_{out} Scholte-Stoneley	c_{out}, a, (d)	Free-field (Proud)	Eq. (26)
S_{in} Scholte-Stoneley	c_{in}, b, (d)	Free-field & Proud	Eq. (27)
r_l internal reflections	c_{in}, b, (d)	Free-field & Proud	Eq. (16)

Table 1 *Summary of selected resonance features, their applicability and related parameters of interest. Reference to corresponding matching models.*

propagation of the outer-fluid-borne waves and on the radiation of the shell-borne waves, depends on the relative impedance between the outer fluid and the bottom: the higher the relative impedance, the more the wave dispersion curves deviate from the corresponding curves computed in the free space.

2.6 Summary of selected waves, related features and matching models

The theoretical investigations on scattering from thin-walled fluid-filled shells lead to:

1. Selection of a set of waves characterizing the scattered response of an elastic shell,
2. Analysis of their frequency behavior in terms of target elastic properties and hence,
3. Formulation of the analytical laws governing the wave characteristics.

The wave families selected for feature extraction are listed in Table 1 with main geometrical and geophysical parameters and reference to the analytical relation model. Among the cited parameters, d sometimes appears in brackets, which means that even if the matching equation used does not depend explicitly on d, the family exists or the related equation is valid only in the case of thin shells. When the equation describing a certain family is considered less reliable when the target lies proud on the seabed than in the free space (see Subsection 2.5), *Proud* is parenthetical.

3

Method of target response analysis

The approach proposed in [4] is extended to fluid-filled shell analysis by introducing the features selected and characterized in Section 2 and a multiple-hypothesis automatic method of resonance identification. The method starts from the assumption that the scatterer is a circular, thin-walled shell insonified at broadside.

A block diagram including the main algorithm steps is provided in Fig. 15. As proposed in [4], a deconvolution phase followed by AR modeling is applied to the target time response. With respect to the method used in [4], only the global response is analyzed here as for proud target real data, the time response length N is usually too short to allow high-resolution spectral representation. Among the estimated AR poles, those located in an annulus defined on the z-plane around the unit circle ($0.95 \leq |z| \leq 1$) are considered resonances. By definition, a pure resonance corresponds to a pole located *on* the unit circle. However, selecting as resonances the poles located in the defined annulus, is justified by two main reasons. As the scattered waves giving rise to resonances are supposed to be attenuated (in Section 2), damped resonance modes are generated, which correspond to z-poles with modulus less than unity. the pole estimation is expected to be affected by a certain error, which is accepted if the resonance pole remains located within the annulus.

The extracted set of resonance frequencies $\left\{f_k^{AR},\ k = 1, .., K\right\}$ are identified by the following automatic technique. The assumption for resonance identification is that the inner fluid is a liquid, hence all the wave families selected in Section 2 are expected to be evident in the scatterer TF.

As the approximated equations referenced in Table 1 are adopted, the location of all the assumed resonance frequencies depend only on the four target parameters a, b, c_{in}, c_*, assuming that the outer fluid sound speed c_{out} is known *a priori*. A range of values for each target parameter (a, b, c_{in}, c_*) is selected, so that a 4D discrete space of possible solutions is built. Each point $\vec{v}$ of this space is a hypothesis uniquely related to a pattern of resonance frequencies by the proposed matching models. The best fit between each pattern and the AR-based extracted resonances is computed by minimizing a distance-based cost functional and providing the estimate $\hat{\vec{v}}$.

Each wave family in the 6-element set $\{S_0,\ S_{out},\ S_{in},\ r_1,\ r_2,\ r_3\}$ is indexed by an

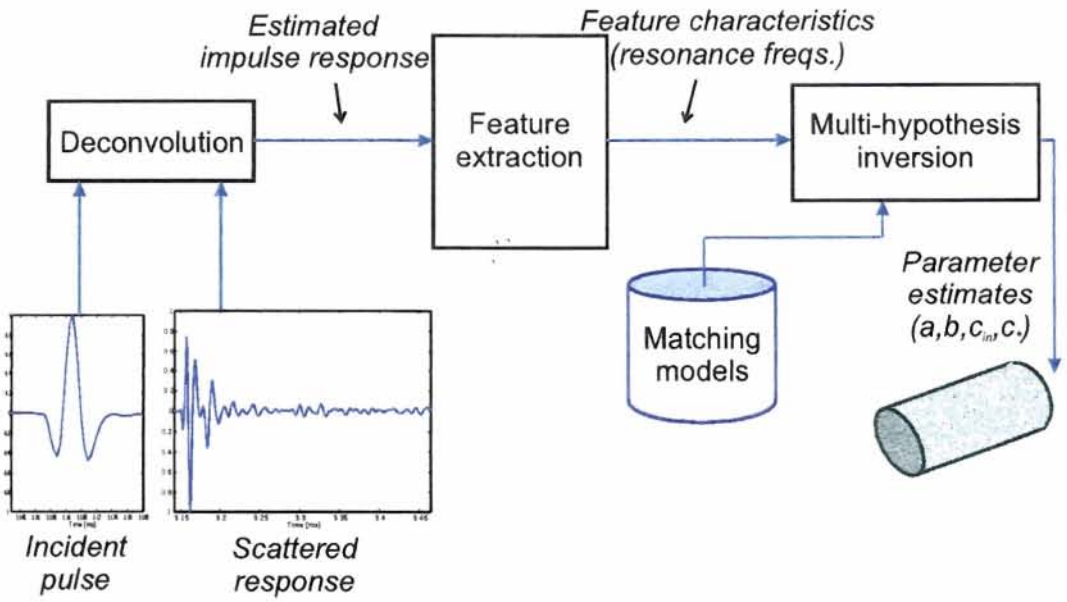

Figure 15 *Block diagram of the main steps of scattering data analysis.*

integer label l ($l \in L = \{1,..,6\}$). For each hypothesis $\vec{v}$ and each family l, the resonance pattern

$$\{f_{l,n_l}(\vec{v}),\ n_l = 1,2,..,N_l\} \tag{32}$$

is built (n_l is the resonance modal order of the l wave type). The association problem is solved by a distance-based approach. The subset of measured resonances $\left\{f^{AR}_{l,\hat{n}_l}(\vec{v}), \hat{n}_l \in \{1,..,N_l\}\right\}$ which best fits the model pattern (Eq. (32)) is found for each family l and for each hypothesis $\vec{v}$ of the space of solutions in terms of minimum Euclidean distance between model-data pairs of frequencies:

$$\left\{f^{AR}_{l,\hat{n}_l}(\vec{v})\right\} = \left\{min_{k,n_l}\left(f^{AR}_{k} - f_{l,n_l}(\vec{v})\right)^2\right\}. \tag{33}$$

For the sake of robustness a wave family is assumed to be detected only if at least three measured resonances are identified as belonging to it.

The estimation result is the parameter vector $\hat{\vec{v}} = \left(\hat{a}, \hat{b}, \hat{c}_{in}, \hat{c}_*\right)$ which minimizes the cost functional:

$$C(\vec{v}) = \sum_{l} \sum_{\hat{n}_l} \left(f^{AR}_{l,\hat{n}_l}(\vec{v}) - f_{l,\hat{n}_l}(\vec{v})\right)^2. \tag{34}$$

The identified resonances corresponding to the $\hat{\vec{v}}$ estimate are collected in the set $\left\{f^{AR}_{\hat{l},\hat{n}_{\hat{l}}}\left(\hat{\vec{v}}\right)\right\}$. The main processing steps summarized in Fig. 15 are amplified in Fig. 16.

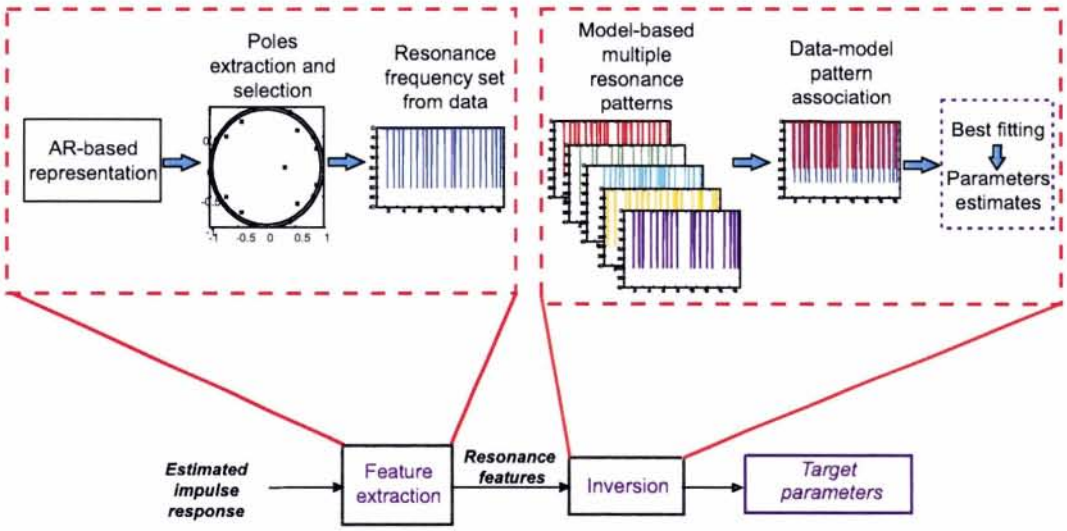

Figure 16 *Detailed diagram of the main processing steps.*

If the problem concerns a proud target, the summation is weighted. The terms regarding outer-fluid-borne wave families become less important, as their resonance locations are predicted by less reliable equations:

$$C(\vec{v}) = \frac{W}{1+W}\left(\frac{1}{W}\sum_{\hat{n}_2}\left(f^{AR}_{2,\hat{n}_2}(\vec{v}) - f_{2,\hat{n}_2}(\vec{v})\right)^2 + \sum_{l\neq S_{out}}\sum_{\hat{n}_l}\left(f^{AR}_{l,\hat{n}_l}(\vec{v}) - f_{l,\hat{n}_l}(\vec{v})\right)^2\right), \tag{35}$$

where the S_{out} wave family is indexed with $l = 2$ and W, $W > 1$, is the weight with which the S_{out} resonance identification is penalized.

The conditional standard deviation $\sigma^{\hat{l}}_{\hat{\vec{v}}}$ between the predicted and measured resonance locations is defined for each wave family $\hat{l}$ identified in the data:

$$\sigma^{\hat{l}}_{\hat{\vec{v}}} = \sqrt{\frac{1}{Q_{\hat{l}}-1}\sum_{\hat{n}_{\hat{l}}}\left(f^{AR}_{\hat{l},\hat{n}_{\hat{l}}}\left(\hat{\vec{v}}\right) - f_{\hat{l},\hat{n}_{\hat{l}}}\left(\hat{\vec{v}}\right)\right)^2}. \tag{36}$$

where $Q_{\hat{l}}$ is the total number of resonance frequencies identified as belonging to the $\hat{l}$ wave family.

If no assumed S_{in}, r_1, r_2, r_3 and S_{out} wave families fit the data, the shell is estimated to be either empty or air-filled. Hence the inner fluid sound speed is estimated to tend to zero, but its numerical evaluation can not be provided on the basis of only these selected features. If no resonance family is detected or the estimated standard deviation associates low reliability to the resonance identification result, then the

hypothesis of cylindrical thin-walled shell at broadside, is not confirmed, and target characterization can not be provided.

In the case of targets lying proud on the sea bottom, the interference effects caused by multi-path sound propagation described in Section 2 are expected to influence the performances of the AR-based algorithms used for the resonance extraction in terms of the number of extracted resonances, the accuracy of their localization and the number of spurious resonances. In this case, the robustness of the method is essentially based on two properties:

- The broadband approach, which implies that many resonance frequencies of the same wave type appear in the signal frequency bandwidth
- The redundancy of information provided by all the resonances belonging to the same wave family and by wave families of the same class.

4

Numerical results

This analysis method was tested on real acoustic data scattered by a thin-walled, water-filled steel cylindrical shell. The cylindrical shell has flat ends, 25 cm outer radius a, 6 mm wall thickness d and 2 m length L. This target can be considered as an example of minelike object.

Data from another experiment are also considered. They are the scattered echoes from the same target filled with sea water and lying proud on a low-relief sandy bottom. The shell was insonified at very low grazing angle (well below the estimated sand critical angle).

In both experiments the parametric source array TOPAS was used [21].

4.1 *Free-field data analysis*

The approach was first tested on "free-field" data recorded in a shallow water basin [1]. The TOPAS was positioned $\sim$ 41m from the target. The steel cylindrical shell was suspended at nominal broadside. A receiving hydrophone was positioned on the transmitter-target axis $\sim$ 6m from the target.

Figure 17 shows an example of data-model fitting of the response to a Ricker pulse (with central frequency at 8 kHz) in time and frequency: the target response is compared with the RST-based prediction. Working conditions do not meet all the RST assumptions, as the shell is not of canonical circular cylindrical shape, having two 15cm-diameter plugs and several external hanging structures, not in the free space, but suspended in the water column by two ropes and related coupling. The shell is finite, but the receiver placement provides a good approximation to infinite length for $f > 4$ kHz, where the end effects are negligible [1]. The Signal-to-Noise Ratio (SNR) is estimated at around 20 dB. In the time domain, one of the major model-data discrepancies evident around 2.2-2.3 ms has not yet been interpreted. In frequency, the main mismatching occurs in the response levels at low frequencies ($f > 4.5$ kHz), which might be caused by end effects.

In Fig. 18 the estimated TF spectrum is compared with the corresponding RST-based prediction. The model-data level mismatching at low frequencies is even more

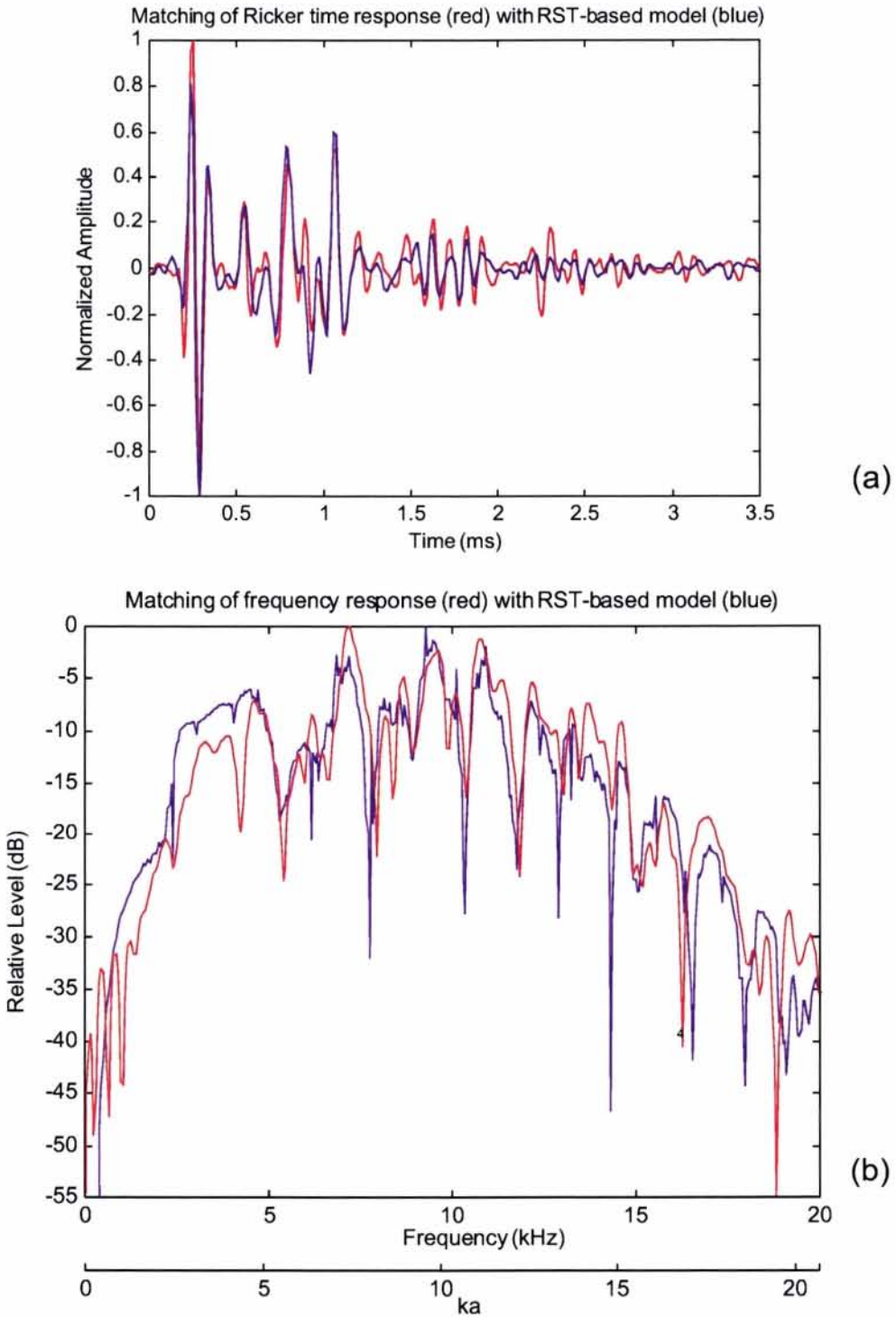

Figure 17 *Model-data fitting of scattering by the water-filled shell in the free-field; target response to a Ricker 8 in (a) time and (b) frequency domains.*

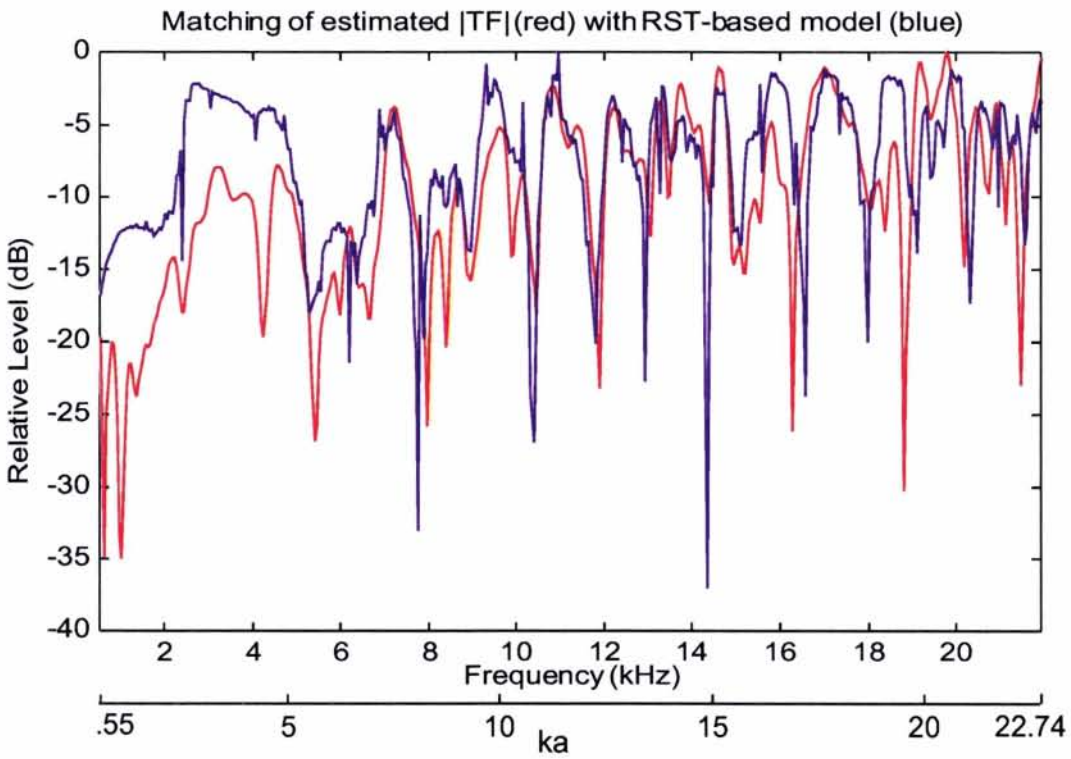

Figure 18 *Model-data curve fitting (TF spectrum) of the water-filled shell in the free field.*

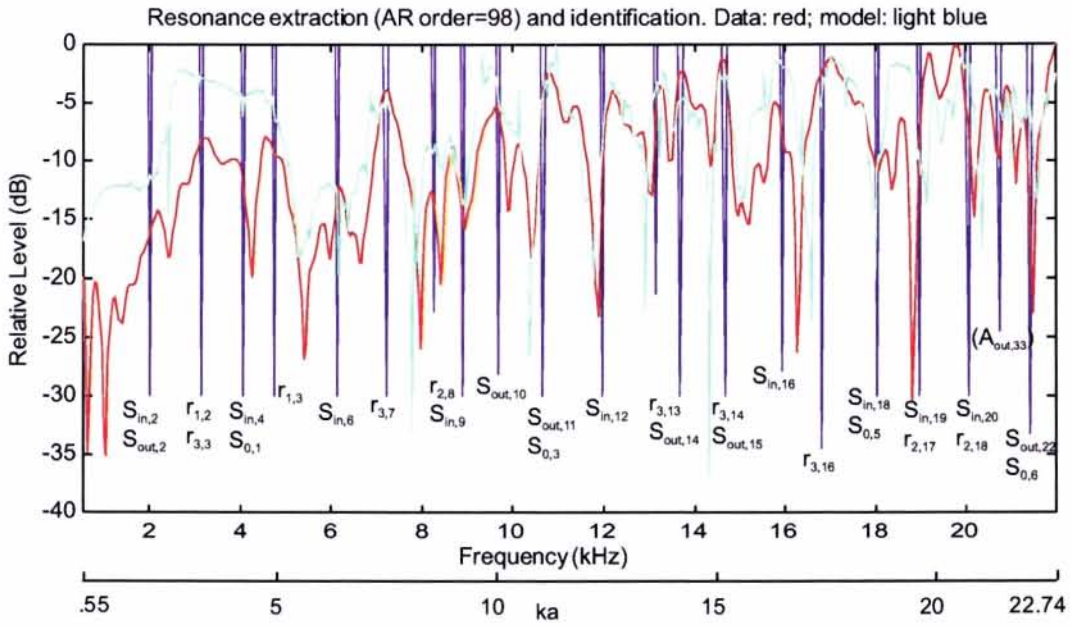

Figure 19 *Resonance extraction and model-based identification.*

evident than in the Ricker response of Fig. 17. Figure 19 shows the same estimated TF spectrum as Fig. 18 where the resonance poles selected by means of the AR-based technique are outlined and identified on the basis of the proposed matching models. The RST-based TF model is shown again as a reference. The curve fitting result is acceptable in terms of dips and peaks; the estimated TF spectral shape and especially its relative amplitude, mismatch the model mainly for $f < 4$kHz where the cylinder end effects, neglected by the model, are expected to be more evident. The AR polynomial order provided by the automatic procedure of parametric spectral estimation proposed in [4] is reported in the plot title. It corresponds to the total number of poles (resonances and not) selected for estimating the scatterer TF on the basis of the acquired data samples. Each resonance label consists of the wave family symbol, indexed by its estimated modal order, i.e., its multiple value. One resonance line can show several labels, as the same location can be shared by resonances belonging to different families.

The adequacy of resonance extraction, interpretation and matching are confirmed by accurate estimates obtained (see Table 2) by the automatic method presented in Section 3. The range of the four unknown parameters provided as input to the estimation procedure are:

- $a \in (20, 30)$cm
- $d \in (0.3, 5)$cm

Parameter	Estimate (σ)	Nominal Value
Outer Radius a [cm]	25.6 (2.5)	25
Thickness d [mm]	4.1 (4)	6
Inner Fluid Speed c_{in} [m/s]	1546 (60)	1528
Shell Speed Parameter c_* [m/s]	5465 (500)	5435

Table 2 *Estimation results obtained from real data of a water-filled steel shell in water (free-field conditions).*

- $c_{in} \in (900, 2000)$m/s
- $c_* \in (3500, 5600)$m/s

Notice that the ranges vary widely, especially those related to c_{in} and c_*. Nevertheless all the parameters are estimated with very good accuracy. The high standard deviation associated with c_* estimate shows low reliability is given to the result.

4.2 Analysis of data from the proud target

The processed data are from sea trials near the northern coast of Elba Island in April '97 in an area characterized by shallow water ($\sim$ 10 m deep) and a fine sand, low-relief bottom. The target was insonified by the TOPAS at nominal broadside, and a 16-element vertical linear array recorded the backscattered echoes. The transmitter and receiver system were located on a 8 m high tower at 40 m from the target. The experimental configuration is similar to that selected for a previous sea trial, in the same coastal area in November 1996 [5].

The target responses used here are the result of a preliminary beamforming phase to separate the target response from the sea surface reflection. The Signal-to-Reverberation Ratio (SRR) estimated from data is around 15 dB. A possible model-data fitting result in terms of time response to a Ricker pulse and TF curve (spectral domain) is presented in Fig. 20. The simulated data are from the free field RST-based model. The model is not perfect as it neglects the bottom. As mentioned in the free-field data analysis, it neglects the cylinder finite-length effects, which could be particularly significant in this case, in which the receiver is in the target far field.

It is evident how the curve fitting result is better in frequency than in time. This can be explained on the basis of the considerations proposed in Section 2.5. The bottom geophysical and geometrical characteristics [5] allow one to assume the existence of a mirror effect. Hence the target response is expected to come from the combination of the responses from the direct and multi-path scattering contributions as introduced in Section 2. In the time domain, the delays predicted between the

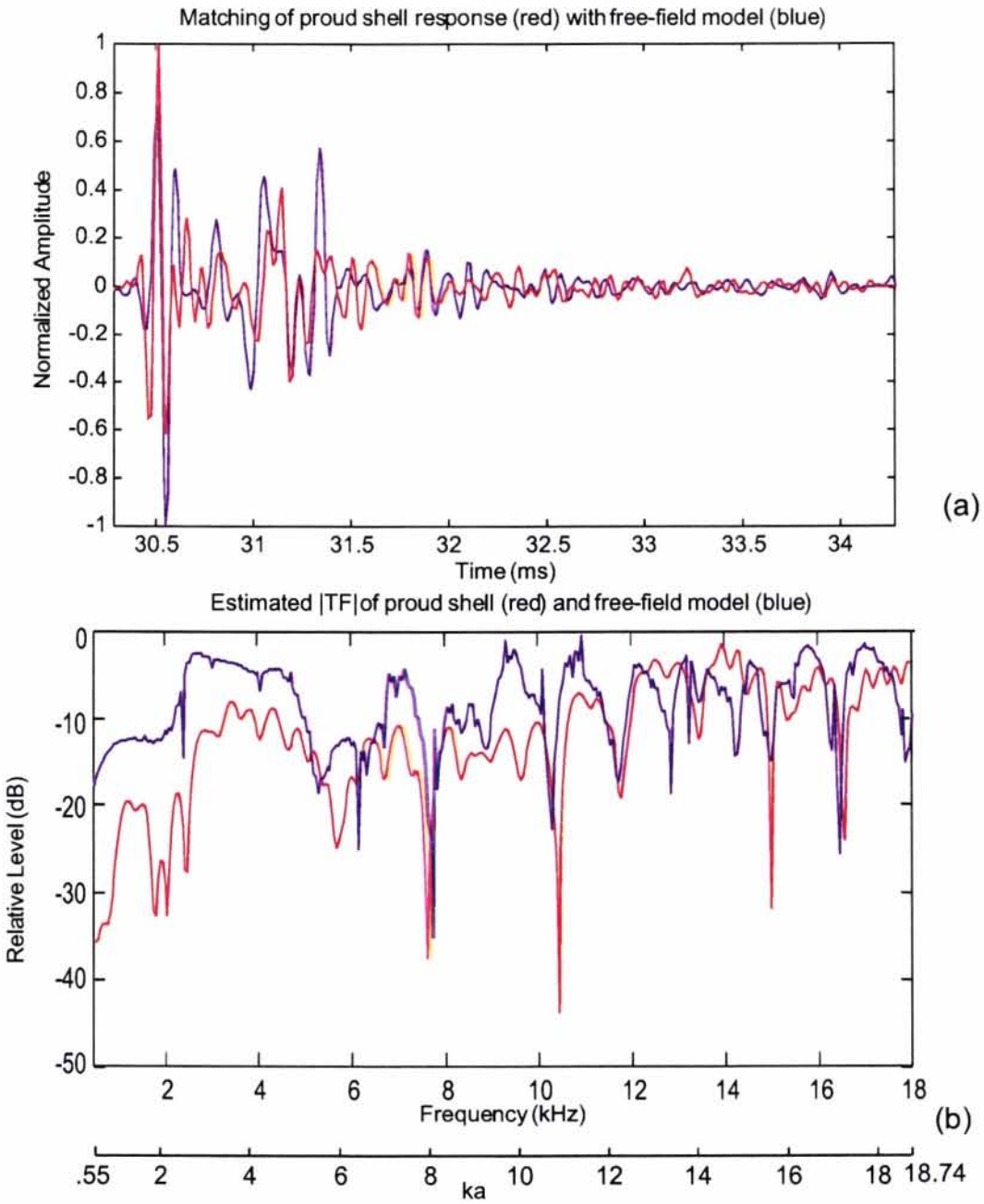

Figure 20 *Model-data fitting of scattering by the proud water-filled shell; time (a) and frequency (b) domain curve fitting.*

direct and bottom-reflected wave paths can give rise to the incoherent superposition of response contributions which is neglected by the free-field RST-based model. In the frequency domain, as predicted, model-data fit is more reasonable and comparable with the result obtained with free-field data, but only in a more limited frequency range. However, the mismatching in terms of spectral level and dip and peak correspondence is locally more significant than in the free-field analysis. The relatively good result obtained in terms of many frequency dips/peaks matching can be justified by considering that:

1. The low grazing angle (about 12°) is assumed to maintain bottom reverberation corrupting the backscattered signal at a low level.

2. The selected grazing angle and the insignificant burial of the target into the seabottom are assumed to have allowed the generation of all the resonance waves expected in the free field and to have maintained their frequency characteristics as predicted by the analytical laws proposed from the plane plate theory.

As in the free-field, a spectral level discrepancy is evident which is spread over a wider frequency range. The cause may be the superposition of end effects with interference between the multi-path response contributions.

The AR-based spectral estimation procedure selects a polynomial order equal to 100 poles from which the resonance frequencies are extracted. Model-data fitting results lead to the interpretation of data in terms of resonance identification. Figure 21 shows the result of the AR-based extraction and the model-based identification of a set of 18 resonance frequencies. The RST-based TF model is shown again as a reference. The result confirms the theoretical predictions. All wave families which are expected to travel either inside the shell or in the inner fluid are identified by some resonances, hence are shown not to change their frequency characteristics. The outer-fluid-borne wave family S_{out} is still detected and identified, which confirms the assumption that its resonance frequency characteristics would have been only slightly affected by the sea bottom.

The inversion results obtained by the automatic parameter estimation method are summarized in Table 3. The same wide ranges of unknown parameter values used in the free-field data analysis are selected here.

With respect to the free-field analysis results, the performance deteriorates in terms of accuracy of the inner fluid speed, particularly in terms of accuracy and reliability of the shell characteristic speed estimates. The main reason is assumed to be the data-model partial mismatching in terms of spectral shape. Mismatching increases after $f = 18$ kHz so that the analysis is limited to the range [2,18] kHz. It can be caused in part by the reverberation effects and in part by the partially disruptive

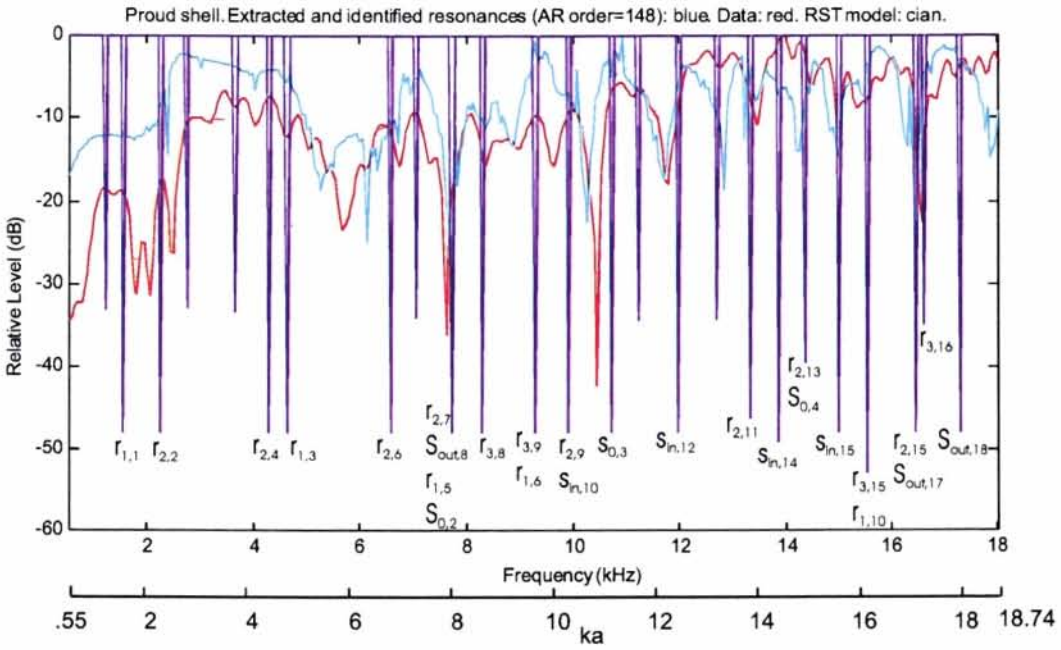

Figure 21 *Resonance extraction and model-based identification.*

Parameter	Estimate (σ)	Nominal Value
Outer Radius a [cm]	24.5 (2.5)	25
Thickness d [mm]	5.9 (5)	6
Inner Fluid Sound Speed c_{in} [m/s]	1600 (50)	1520
Shell Characteristic Speed c_* [m/s]	4845 (500)	5435

Table 3 *Estimation results obtained from real data of a water-filled steel shell lying proud on a sandy sea bottom.*

interference effects occurring at certain frequencies because of multi-path. The effects of the frequency modulation assumed to derive from the interaction with the bottom boundary as proposed in Section 2 can be outlined in terms of changes in the estimated TF spectral level, compared with the free-field model; these amplitude changes are forecast to vary with frequency and, hence, to affect in a significant way the presence and level of some spectral dips/peaks predicted by the model. This deviation of data from the assumed model can imply a significant deterioration in the accuracy of resonance extraction and model-based resonance identification processes. However, the wider the frequency range with good SRR level, where it is possible to apply the analysis, the more this degradation effect can be limited. This emphasizes the importance of the broadband nature of the approach.

Even if the accurate estimation of the two geometrical parameters (i.e., outer radius and thickness) is encouraging and thickness evaluation is a highly discriminating

feature for classification of man-made and natural targets, a refinement of the estimation of two speed parameters could be useful for distinguishing between mines and man-made objects of similar geometry and for identification purposes.

In the free field and in the proud case the number of extracted and processed resonance modes is much lower than the number of resonances one would expect as predicted by the RST-based model in this frequency range. Figures 19 and 21 show cases in which the curve fitting result would outline the presence of sharp peaks or troughs predicted by theory, but not estimated by the automatic technique of resonance extraction and identification. In fact, many resonances are expected to be generated by a fluid-filled shell in this wideband range. Those belonging to the same class of wave types (e.g., the internal reflections of different orders and the inner surface waves) provide redundant information. Hence, selecting and processing only those resonance frequencies extracted and identified with higher accuracy and reliability, is expected to provide better inversion results.

5 Discussion

The AR-based method of acoustic resonance scattering analysis proposed in [4] for processing data scattered by free-field, air-filled or empty cylindrical shells at broadside has been extended to the case of liquid-filled cylindrical shells at broadside. The shell can be made of any solid and filled with any liquid, but must be thin with respect to the wavelength ($fd < 1$ MHz mm). This report has addressed the analysis of scattering by a water-filled, thin-walled cylindrical shell at low-intermediate frequencies ($ka \in (2, 20)$, $fd \leq 0.13$ MHz mm).

Theoretical investigations on a set of periodical wave types traveling around the target and characterization of the backscattering physics have been proposed in the free-space case and then extended to the case of the target lying proud on the seabottom.

The physical interpretation of the behavior of the selected periodical acoustic phenomena in the free space are based on the Plane Plate Theory, Resonance Scattering Theory and Ray Theory. A RST-based simulator of acoustic scattering data has been developed [3]. With respect to the case of air-filled or empty shells the presence of an inner fluid has been shown to add three new families of surface waves to the previous three families and a class of multiple internal reflections of several orders. The selected wave types are inner-fluid-borne, shell-borne and outer-fluid-borne surface waves and periodical internal transmission/reflection waves. Analytical models correlating the dispersion curve characteristics of the selected wave families with the resonance frequencies detected in the scatterer response have been derived from the approximate solution of the free-field problem.

The interpretation of scattering by a target lying on the sea bottom in terms of the same families of periodical waves has been discussed as an extension of the free-space case and is based on the single-scattering model proposed in [5].

An automatic, multi-hypothesis technique of resonance identification in the frequency domain has been developed, which uses matching equations to estimate target geometrical and geophysical parameters from scattering response, at target broadside aspect, given some *a priori* information on the object shape. One of the most significant characteristics of the selected approach is applying *broadband* analysis. This implies that many resonance frequencies of the same wave type and

of different families are located in the used frequency bandwidth. The consequent *redundancy of information* provided by processing all the extracted resonances belonging to the same wave family and by wave families of the same class is expected to improve robustness.

The method has been tested on real data scattered by the same water-filled cylindrical shell either submerged in roughly free space or lying proud on a sandy seabed. The data have been evaluated with high SNR values. Processing data with high SNR levels has allowed the evaluation of feasibility and capabilities of the new approach proposed. The evaluation of the method sensitivity to noise and reverberation will be considered in a future study. The method performances have been shown in terms of fit between theory and experiment, and numerical results.
Good results in terms of TF curve fitting and in particular of estimated parameters have been obtained from the recorded "free-field" data. They have confirmed the adequacy of the scattering model used notwithstanding the approximations introduced. In particular, the method, based on the theoretical interpretation of scattering by an *infinite shell of a canonical circular cylindrical shape in the free field* has provided good performance when applied to data scattered by a *finite* target which has cylindrical shape but several external frames for suspension and two plugs, and which was kept underwater under "free-field" conditions by two ropes and related steel coupling.

For data scattered by proud targets, the performance deterioration expected by using free-space modeling in the presence of a boundary, is confirmed by inferior results, in particular in terms of inversion.

The selected low grazing angle allows relatively low reverberation levels. Model-data fit of the target spectral response has been considered acceptable in the analyzed frequency range despite some local mismatching, which can lead to significant operational consequences. However, the reverberation may have contributed to local model-data mismatching which have affected the results of resonance extraction and identification. It has also made it necessary to limit the broadband frequency range analyzed from [2,22] to [2,17] kHz. As broadband analysis and accuracy of resonance extraction are among the key points of the proposed approach, the reverberation sensitivity of the method is considered one of its main limitations.

From an accurate comparison of the spectral shape of the free-field model with the proud-target data, the following considerations validate the physical interpretation. The contact of the target with the sandy bottom boundary has little effect on resonance frequency characteristics in terms of wave dispersion curves, which consequently, can still be predicted by free-space plane-plate theory and resonance scattering theory. This could depend also on the negligible burial depth of the target,

for which the area of the target-sediment interface is very small compared to that of the target-water interface. The characteristics of the scattering waves traveling in the outer fluid would significantly change with the target burial depth.

It is suggested that a frequency modulation effect on the direct-path-only transfer function of the target, is caused by sound interaction with the bottom boundary multi-path. It may have contributed to locally poor model-data fit by influencing the detectability of the resonance frequencies expected on the basis of the free-space modeling. The modulation effects vary with grazing angle and frequency, but seem not to cause changes in the pattern of resonance frequency locations in the spectral domain. Even when some of the resonance spectral dips or peaks are not detectable because of completely disruptive interferences among the multi-path contributions, the method robustness would be enhanced by the selected *broadband approach* and the consequent *redundancy of information* provided by some of the extracted resonances.

The proposed interpretation of scattering phenomena in the proud-target case is validated on too limited a set of data to be able to draw final conclusions. Extended sets of measurements of scattering by the same proud target insonified with varying grazing angles and different types of bottom sediments would be useful for validating the proposed interpretation and defining the limits of the model applicability. To this end, comparing the scattering response by the target when lying proud on the sea bottom and when partially buried at various depths could be useful.

The approach appears to work best with the target in free field, and suffers a certain performance degradation for targets proud on the sea bottom, even when insonified at low grazing angles.
Under these conditions, the current main constraints imposed for the method applicability consist in *a priori* knowledge on:

1. Target shape (only circular cylindrical thin-walled shells),
2. The target aspect (only at broadside),
3. Ranges of values for the target unknown parameters (used as search bounds for the multi-hypothesis estimation method).

The method has been applied with wide ranges of search, in particular of the unknown inner fluid and shell material sound speeds. Inversion results could improve if these search bounds were restricted.

Future work will consist of

- A feasibility study and evaluation of the capabilities of resonance-based analysis of data scattered by buried objects.
- Multiple-aspect resonance scattering analysis and fusion of resonance analysis with multiple-aspect approaches, such as tomography.

A multiple-aspect approach is expected to allow one to:

- Work with data scattered at aspects different from broadside (constraint 2.),
- Produce analyses which are robust to noise and more accurate, thanks to the partially redundant information contained in the target response when recorded at different aspects.

Fusion with other multi-aspect techniques able to provide a rough estimation of the object external shape, dimensions and orientation would allow relaxation of constraint 3.

The extension to more complex man-made targets and their classification against natural objects is also forecast.

6

Acknowledgements

This work was partially funded by the European Union as part of the MAST-III Project: Detection of Embedded Objects (DEO).

References

[1] W. L. J. Fox, J. A. Fawcett, D. Jourdain-Albonico, and A. Tesei, "Measurements of free-field acoustic scattering from cylindrical shells," SM-331, SACLANT Undersea Research Centre, La Spezia, Italy, May 1997.

[2] N. D. Veksler, *Resonance Acoustic Spectroscopy.* Berlin: Springer Verlag, 1993.

[3] L. Flax, L. R. Dragonette, and H. Überall, "Theory of elastic resonance excitation by sound scattering," *Journal of the Acoustical Society of America*, vol. 63, pp. 723–731, March 1978.

[4] A. Tesei, W. L. J. Fox, A. Maguer, and A. Løvik, "Resonance scattering analysis by autoregressive models applied to air-filled, cylindrical, thin-walled shells in water," SR-265, SACLANT Undersea Research Centre, La Spezia, Italy, Oct. 1997.

[5] J. A. Fawcett, W. L. J. Fox, and A. Maguer, "Modelling of acoustic scattering by objects on the seabed," SR-276, SACLANT Undersea Research Centre, La Spezia, Italy, Oct. 1997.

[6] J. A. Fawcett, "Modelling scattering from partially buried objects," SM-320, SACLANT Undersea Research Centre, La Spezia, Italy, Dec. 1996.

[7] S. M. Kay, *Modern Spectral Estimation: Theory and Application.* New York: Prentice Hall, 1988.

[8] M. Talmant and G. Quentin, "Backscattering of a short ultrasonic pulse from thin cylindrical shells," *Journal of Applied Physics*, vol. 63, pp. 1857–1863, March 1988.

[9] K. L. Williams and P. L. Marston, "Backscattering from an elastic sphere: Sommerfeld-Watson transformation and experimental confirmation," *Journal of the Acoustical Society of America*, vol. 78, pp. 1093–1102, Aug. 1985.

[10] A. Derem, J. L. Rousselot, G. Maze, J. Ripoche, and A. Faure, "Diffusion d'une onde acoustique plane par des cylindres solides immerges: etude experimentale et theorie des resonances," *Acustica*, vol. 50, pp. 39–50, 1982.

[11] J. Dickey, G. Maidanik, and H. Überall, "The splitting of dispersion curves for the fluid-loaded plate," *Journal of the Acoustical Society of America*, vol. 98, pp. 2365–2367, Oct. 1995.

[12] J.-P. Sessarego, J. Sageloli, C. Gazanhes, and H. Überall, "Two Scholte-Stoneley waves on doubly fluid-loaded plates and shells," *Journal of the Acoustical Society of America*, vol. 101, pp. 135–142, Jan. 1997.

[13] M. F. M. Osborne and S. D. Hart, "Transmission, reflection, and guiding of an exponential pulse by a steel plate in water. i. Theory," *Journal of the Acoustical Society of America*, vol. 17, pp. 1–18, July 1945.

[14] G. Quentin and M. Talmant, "The plane plate model applied to the scattering of the ultrasonic waves from cylindrical shells," in *Elastic wave propagation* (M. F. McCarthy and M. A. Hayes, eds.), pp. 477–482, Elsevier Science, North-Holland, 1989.

[15] M. L. Rumerman, "Contribution of membrane wave reradiation to scattering from finite cylindrical steel shells in water," *Journal of the Acoustical Society of America*, vol. 93, pp. 55–65, January 1993.

[16] H. Überall, B. Hosten, M. Deschamps, and A. Gerard, "Repulsion of phase-velocity dispersion curves and the nature of plate vibrations," *Journal of the Acoustical Society of America*, vol. 96, pp. 908–917, Aug. 1994.

[17] J.-P. Sessarego, J. Sageloli, P. Degoul, P. Flandrin, and M. Zakharia, "Analyse temps-frequence de signaux en milieux dispersifs. Application a l'etude des ondes de Lamb," *Journal de Acoustique*, vol. 3, pp. 273–280, Sept. 1990.

[18] L. M. Brekhovskikh and O. Godin, *Acoustics of Layered Media I.* Berlin: Springer Verlag, 1990.

[19] A. Maguer, E. Bovio, W. L. J. Fox, E. Pouliquen, and H. Schmidt, "Mechanisms for subcritical angle penetration into a sandy bottom: Experimental and modeling results," SR-287, SACLANT Undersea Research Centre, La Spezia, Italy, in press 1998.

[20] F. B. Jensen, W. A. Kuperman, M. B. Porter, and H. Schmidt, *Computational Ocean Acoustics.* New York: AIP Press, 1994.

[21] Bentech Subsea AS, Stjørdal, Norway, *Simrad TOPAS PS 040 Operator Manual.*

Annex A

The steady-state 2D wave-guide problem

The behavior of steady-state scattering of a plane wave by a fluid-loaded, plane, thin plate is studied by solving the 2D wave-guide problem. The problem can be stated as follows. Find the potentials ϕ_1, ϕ and ψ, and ϕ_2 of the displacements in fluid 1, plate and fluid 2 respectively, that satisfy the wave equations:

- in fluid 1:

$$\left(\nabla^2 - \frac{1}{c_1^2}\frac{\partial^2}{\partial t^2}\right)\phi_1 = 0; \tag{A1}$$

- in the plate:

$$\begin{aligned}\left(\nabla^2 - \tfrac{1}{c_p^2}\tfrac{\partial^2}{\partial t^2}\right)\phi = 0,\\ \left(\nabla^2 - \tfrac{1}{c_s^2}\tfrac{\partial^2}{\partial t^2}\right)\psi = 0;\end{aligned} \tag{A2}$$

- in fluid 2:

$$\left(\nabla^2 - \frac{1}{c_2^2}\frac{\partial^2}{\partial t^2}\right)\phi_2 = 0. \tag{A3}$$

The plate displacement is defined as:

$$\begin{aligned}u &= \tfrac{\partial\phi}{\partial x} + \tfrac{\partial\psi}{\partial z},\\ v &= \tfrac{\partial\phi}{\partial z} - \tfrac{\partial\psi}{\partial x}.\end{aligned} \tag{A4}$$

in the x and z directions respectively. The displacement in fluid 1 is defined as:

$$\begin{aligned}u &= \tfrac{\partial\phi_1}{\partial x},\\ v &= \tfrac{\partial\phi_1}{\partial z}.\end{aligned} \tag{A5}$$

in the x and z directions respectively. The displacement in fluid 2 is:

$$\begin{aligned}u &= \tfrac{\partial\phi_2}{\partial x},\\ v &= \tfrac{\partial\phi_2}{\partial z}.\end{aligned} \tag{A6}$$

The boundary conditions at $z = \pm d/2$ are expressed in terms of the stresses $(p_{zz})_1$, $(p_{zz})_2$, p_{zz} and p_{xz}, defined in the respective media as:

$$\begin{aligned}
(p_{zz})_1 &= \lambda_1 \left(\frac{\partial u}{\partial x} + \frac{\partial v}{\partial z} \right), \\
(p_{zz})_2 &= \lambda_2 \left(\frac{\partial u}{\partial x} + \frac{\partial v}{\partial z} \right), \\
p_{zz} &= \lambda \left(\frac{\partial u}{\partial x} + \frac{\partial v}{\partial z} \right) + 2\mu \frac{\partial v}{\partial z}, \\
p_{xz} &= \mu \left(\frac{\partial v}{\partial x} + \frac{\partial u}{\partial z} \right);
\end{aligned} \tag{A7}$$

where λ and μ are Lamé's constants which can be expressed in terms of the medium sound speed(s) and density:

$$\begin{aligned}
\mu &= \tfrac{\rho}{c_s^2}, \\
\lambda &= \rho c_p^2 - 2\mu.
\end{aligned} \tag{A8}$$

Hence $\mu = 0$ in fluids. In this work Poisson's hypothesis is assumed for the plate, for which $\lambda \approx \mu$, hence $c_p^2 \approx 3c_s^2$. The boundary conditions to satisfy are:

1. p_{zz} continuous at $z = \pm d/2$;
2. p_{xz} vanishes at $z = \pm d/2$;
3. v continuous at $z = \pm d/2$.

The solution must be of the form $f(x,z)\exp^{j\omega t}$, with $\omega = 2\pi f$. The variables are assumed separable, the separation constants being $-k_{z,1}^2, -k_{z,p}^2, -k_{z,s}^2, -k_{z,2}^2$ in z, and $-k_{ph}^2$ in x (see their reciprocal relations in Eq. (4)). The x separation constant must be unique for all the potentials for respecting the steady-state condition along x. Moreover, assuming only progressive waves, the k_{ph} sign is fixed to $+$. Hence the solutions can be expressed as follows:

$$\begin{aligned}
\phi_1 &= A_1 e^{j\, k_{z,1} z} e^{j(\omega t + k_{ph} x)}; \\
\phi &= \left(A_p cosh(j k_{z,p} z) + B_p sinh(j k_{z,p} z) \right) e^{j(\omega t + k_{ph} x)}; \\
\psi &= \left(A_s cosh(j k_{z,s} z) + B_s sinh(j k_{z,s} z) \right) e^{j(\omega t + k_{ph} x)}; \\
\phi_2 &= A_2 e^{-j\, k_{z,2} z} e^{j(\omega t + k_{ph} x)};
\end{aligned} \tag{A9}$$

If the assumed solutions are substituted into the imposed boundary conditions a linear system in the variables A_1, A_p, A_s, B_p, B_s and A_2 is built in the form $\mathbf{C}\,\mathbf{x} = \mathbf{0}$, where $\mathbf{x} = [A_1\ A_p\ A_s\ B_p\ B_s\ A_2]^T$, $\mathbf{0}$ is a six-zero vector, and the 6x6

coefficient matrix $\mathbf{C}$ follows (subdivided into three columns per line):

$$\mathbf{C} = \begin{bmatrix} 0 & k_{z,p}\alpha & -k_{ph}\beta \\ -k_{z,1}e^{-jk_{z,1}\frac{d}{2}} & -k_{z,p}\alpha & -k_{ph}\beta \\ 0 & \mu(k_{ph}^2 - k_{z,s}^2)\gamma & 2\mu k_{ph}k_{z,s}\xi \\ \lambda_1 e^{-jk_{z,1}\frac{d}{2}}(k_{ph}^2 + k_{z,1}^2) & \mu(k_{ph}^2 - k_{z,s}^2)\gamma & -2\mu k_{ph}k_{z,s}\xi \\ 0 & 2k_{ph}k_{z,p}\alpha & (k_{ph}^2 - k_{z,s}^2)\beta \\ 0 & -2k_{ph}k_{z,p}\alpha & (k_{ph}^2 - k_{z,s}^2)\beta \end{bmatrix}$$

$$\begin{bmatrix} k_{z,p}\gamma & -k_{ph}\xi & k_{z,2}e^{-jk_{z,2}\frac{d}{2}} \\ k_{z,p}\gamma & k_{ph}\xi & 0 \\ \mu(k_{ph}^2 - k_{z,s}^2)\alpha & 2\mu k_{ph}k_{z,s}\beta & \lambda_2 e^{-jk_{z,2}\frac{d}{2}}(k_{ph}^2 + k_{z,2}^2) \\ -\mu(k_{ph}^2 - k_{z,s}^2)\alpha & 2\mu k_{ph}k_{z,s}\beta & 0 \\ -2k_{ph}k_{z,p}\gamma & -(k_{ph}^2 - k_{z,s}^2)\xi & 0 \\ -2k_{ph}k_{z,p}\gamma & (k_{ph}^2 - k_{z,s}^2)\xi & 0 \end{bmatrix} \tag{A10}$$

where

$$\begin{aligned} \alpha &= sinh(jk_{z,p}\tfrac{d}{2}) \\ \beta &= cosh(jk_{z,s}\tfrac{d}{2}) \\ \gamma &= cosh(jk_{z,p}\tfrac{d}{2}) \\ \xi &= sinh(jk_{z,s}\tfrac{d}{2}) \end{aligned} \tag{A11}$$

The common factor $e^{j(\omega t + k_{ph}x)}$ has been cancelled from every equation. A solution of the system exists if the determinant of the coefficient matrix vanishes. This condition gives rise to the general characteristic equation provided in Eq. (2).

In the particular case of two identical fluids loading the plate, the symbols $k_{z,fl} = k_{z,1} = k_{z,2}$ and $\lambda_{fl} = \lambda_1 = \lambda_2$ are introduced, and the determinant can be arranged in the form

$$\begin{vmatrix} M_1 & 0 \\ 0 & M_2 \end{vmatrix} \tag{A12}$$

where

$$M_1 = \begin{bmatrix} k_{z,fl}e^{-jk_{z,fl}\frac{d}{2}} & k_{z,p}\alpha & -k_{ph}\xi \\ (k_{ph}^2 + k_{z,fl}^2)\frac{\lambda_{fl}}{\mu}e^{-jk_{z,fl}\frac{d}{2}} & (k_{ph}^2 - k_{z,s}^2)\gamma & 2k_{ph}k_{z,s}\beta \\ 0 & 2k_{ph}k_{z,p}\alpha & -(k_{ph}^2 - k_{z,s}^2)\alpha \end{bmatrix}, \tag{A13}$$

$$M_2 = \begin{bmatrix} k_{z,fl}e^{-jk_{z,fl}\frac{d}{2}} & k_{z,p}\gamma & -k_{ph}\beta \\ (k_{ph}^2 + k_{z,fl}^2)\frac{\lambda_{fl}}{\mu}e^{-jk_{z,fl}\frac{d}{2}} & (k_{ph}^2 - k_{z,s}^2)\alpha & 2k_{ph}k_{z,s}\xi \\ 0 & -2k_{ph}k_{z,p}\gamma & (k_{ph}^2 - k_{z,s}^2)\gamma \end{bmatrix}. \tag{A14}$$

If $A_1 = A_2$ is chosen, the global determinant corresponds to the upper diagonal minor M_1 which corresponds to Eq. (6), if the definitions expressed by Eq. (4) are used. In

this case the remained four functions describe a motion of the plate *symmetric* with respect to its median plane. Alternatively, $A_1 = -A_2$ is fixed, in which case the lower diagonal minor M_2 is found as global determinant and the second equation of (6) derives, which describes a motion of the plate *antisymmetric* with respect to its median plane. At low frequencies (i.e., thin plates) the symmetric and antisymmetric functions describe the longitudinal and flexural vibrations of the plate, respectively. Hence, the convenient form of the determinant shown in Eq. (A12) simplifies the discussion of the two classes of waves, as presented in subsection 2.2.1.

Report no. changed (Mar 2006): SR-295-UU

Document Data Sheet

Security Classification		Project No.
		031-2/033-3
Document Serial No.	**Date of Issue**	**Total Pages**
SR-295	September 1998	59 pp.

Author(s)

Tesei, A., Fawcett, J.A., Fox, W.L.J., Maguer, A.

Title

Resonance analysis of the acoustic response of a water-filled cylindrical shell.

Abstract

Resonance analysis of the acoustic response of a water-filled cylindrical shell.

The resonance analysis approach developed for characterizing free-field air-filled cylindrical shells in terms of geometrical and mechanical parameters is extended to fluid-filled shells either in the free-field or proud on the sea bottom.

The resonance phenomena generated when a target is insonified at broadside, by broadband, low-frequency, incident pulses are investigated in the *ka* range (2,25). Attention is focused on those scattering phenomena common to free-field and proud cases. A comparison is also drawn between the resonance behaviour of the same cylindrical target filled with either air or sea water. From the study of a set of fluid-borne and shell-borne wave families, equations are formulated which relate their characteristics to the target elastic properties. Resonance frequencies are detected and localized by the algorithm presented earlier, identified and used for parameter estimation by an automatic multi-hypothesis method of model-data fitting. The approach was tested on real acoustic data backscattered by a water-filled finite cylinder either suspended in free-field, or lying proud on a sandy sea bottom and insonified at very low grazing angle (below the seabed critical angle). A good agreement between theory and experiment was found in terms of model-data fit and target parameter estimates.

The results achieved encourage the extension of target echo analysis to objects buried in bottom sediment. The extension to multi-aspect resonance scattering analysis of the same and more complex objects is also planned.

Keywords

Issuing Organization

North Atlantic Treaty Organization
SACLANT Undersea Research Centre
Viale San Bartolomeo 400, 19138 La Spezia, Italy

[From N. America: SACLANTCEN (New York) APO AE 09613]

Tel: +39 0187 527 361
Fax:+39 0187 524 600

E-mail: library@saclantc.nato.int

Report no. changed (Mar 2006): SR-295-UU

Initial Distribution for Unclassified SR-295

Ministries of Defence

DND Canada	10
CHOD Denmark	8
DGA France	8
MOD Germany	15
HNDGS Greece	12
MARISTAT Italy	9
MOD (Navy) Netherlands	12
NDRE Norway	10
MOD Portugal	5
MDN Spain	2
TDKK and DNHO Turkey	5
MOD UK	20
ONR USA	34

NATO Commands and Agencies

NAMILCOM	2
SACLANT	3
CINCEASTLANT/ COMNAVNORTHWEST	1
CINCIBERLANT	1
CINCWESTLANT	1
COMASWSTRIKFOR	1
COMSTRIKFLTANT	1
COMSUBACLANT	1
SACLANTREPEUR	1
SACEUR	2
CINCNORTHWEST	1
CINCSOUTH	1
COMEDCENT	1
COMMARAIRMED	1
COMNAVSOUTH	1
COMSTRIKFORSOUTH	1
COMSUBMED	1
NC3A	1
PAT	1

Scientific Committee of National Representatives

SCNR Belgium	1
SCNR Canada	1
SCNR Denmark	1
SCNR Germany	1
SCNR Greece	1
SCNR Italy	1
SCNR Netherlands	2
SCNR Norway	1
SCNR Portugal	1
SCNR Spain	1
SCNR Turkey	1
SCNR UK	1
SCNR USA	2
French Delegate	1
SECGEN Rep. SCNR	1
NAMILCOM Rep. SCNR	1

National Liaison Officers

NLO Canada	1
NLO Denmark	1
NLO Germany	1
NLO Italy	1
NLO Netherlands	1
NLO Spain	1
NLO UK	1
NLO USA	1

Sub-total	199
SACLANTCEN	30
Total	229